R 635

Technical Report

OCEAN SEDIMENT HOLDING STRENGTH AGAINST BREAKOUT OF EMBEDDED OBJECTS

August 1969

Sponsored by

DEEP SUBMERGENCE SYSTEMS PROJECT OFFICE

U. S. NAVAL CIVIL ENGINEERING LABORATORY

Port Hueneme, California

OCEAN SEDIMENT HOLDING STRENGTH AGAINST BREAKOUT OF EMBEDDED OBJECTS

Technical Report R-635

56-001

by

Cheng L. Liu

ABSTRACT

This report concludes 3 years of breakout force research. The third phase of the field test conducted in the Gulf of Mexico and a small-scale model study are described. All of the experimental results are presented in a new dimensionless correlation (between breakout force and breakout time) based on the mechanism of the breakout. The mean soil holding strength (F_m) is considered to depend upon average soil cohesion, object geometry, the time the object has been embedded (T_{in}), and the time allowed for pull-out (T):

$$\frac{F_m}{F_r} = 1.5 \left(\frac{T}{T_{in}}\right)^{-0.07} \qquad \text{for } 10^{-3} < T/T_{in} < 10$$

where F_r is the static soil resistance due to shear and tension. An example is also presented to illustrate the application of this equation. The small-scale model test is considered a useful tool in obtaining more data in future research.

CONTENTS

INTRODUCTION

General Problem

Breakout force is the force required to lift an object from the ocean bottom soil in a specified time minus the submerged weight of the object. Sometimes the breakout force is referred to as the "mud suction." Foundation engineers are interested in the settlement of structures on dry land, and salvage engineers are troubled by the extrication of objects from the saturated ocean bottom. Although these two problems are not exactly the same, they have several things in common. First, both phenomena are time dependent. Structures may take years to settle, but a breakout operation may last at most a few days, and usually only several hours, unless the object never breaks out at all. Second, they both take place through the soil surface. Third, they are subject to a vertical driving force, such as the weight of the object.

Before a heavy object, such as a sunken submarine, is lifted from the ocean bottom, a reasonable estimate of the required breakout force would eliminate the loss of time and equipment during the actual operation. However, as in the case of object settlement, the breakout force is not the only controlling parameter. Another dominant parameter is the period of time that the breakout force must be applied to achieve the detachment of the object from the soil. Either parameter can be specified and the other one estimated.

In a submarine rescue mission, the breakout time is limited by the submarine emergency life support capacity, and an immediate breakout may be required. The breakout force necessary to lift the submarine within a specified time should be estimated before the rescue mission. In case this breakout force is too large for the lifting capacity of the surface ship, means of reducing the breakout force must be employed. Pivoting the sunken object or jetting under its hull are methods commonly used. Even oscillating the applied force would speed up the breakout. But the effectiveness of each of these methods has not been evaluated. On the other hand, a submersible design engineer would be interested in knowing the minimum propulsion power required for the submersible to break loose from the bottom mud after resting on it for a period of time.

Since breakout has not been a problem on dry land and its importance in ocean engineering has only recently been realized, little knowledge concerning the breakout phenomenon can be found in soil mechanics literature. Only traces of salvage experience are recorded here and there in ships' logs. The mechanism of the breakout phenomenon is not today clearly understood.

This report includes the data obtained from the third phase of the testing program in the Gulf of Mexico. Supplementary model test data are presented. A final analysis of the data and a discussion of the reliability of the empirical formula are also included. And, finally, the utilization of the test results is illustrated by an example.

Past Work at NCEL

A 3-year analytical and experimental study, sponsored by the Deep Submergence Systems Project, has been undertaken by NCEL since July 1965. The main objectives of the study are (1) to develop a technique for estimating the breakout force or time for objects of various size, shape, and skin roughness embedded in ocean bottom soils, (2) to specify the possible error of such a technique, and (3) to investigate the effectiveness of various means of reducing soil holding strength.

Field Tests. In order to obtain enough data for the derivation of an empirical formula for the prediction of breakout force, large-scale field tests have been conducted. The first two phases of the experimental work were carried out at Seal Beach, California, and in the San Francisco Bay.

In the first year of the study, work included the first phase of the field tests and the formulation of an analytical method. The preliminary field test program was designed to obtain as much information as possible in a simulated ocean bottom soil. Tests were conducted in a mud pit 36 feet in diameter and 16 feet in depth. The soil was borrowed from a nearby swamp area. Its properties were highly variable with respect to the sampling location inside the pit. Objects of various shapes and sizes were tested in this pit. A crane was first used to pull the object out at a constant rate, and later a counterweight balance method was employed to provide a constant pulling force. The objects were forced into the soil instead of being allowed to sink of their own weight. The test setup is shown in Figure 1. Note the method used to apply a constant load. An attempt was made to correlate the Euler number with the Reynolds number. This correlation was difficult to achieve because of the difficulty in measuring soil viscosity. Methods of reducing soil resistance were tested. A detailed test description and data presentation may be found in Reference 1.

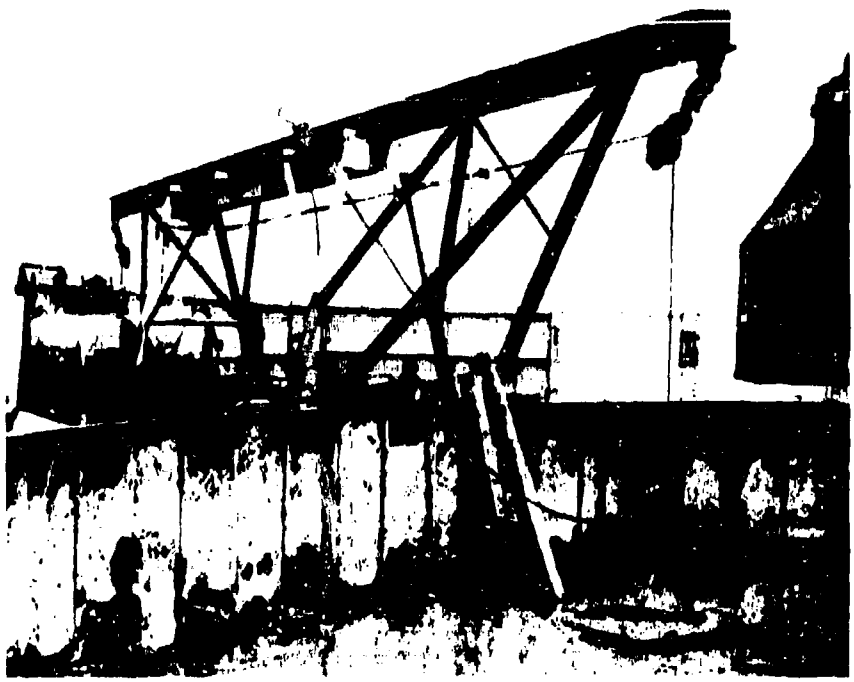

Figure 1. Seal Beach breakout test facility.

The second year's progress consisted of shallow-water field tests in the San Francisco Bay. The field tests were conducted under about 30 feet of seawater. The bottom soil consisted of silty clay with pockets of sand and shells. The lifting force was provided by a counterweight from a moored barge. Figure 2 shows the mooring and the testing arrangement of the equipment. The force, which was varied by adjusting the amount of water in the counterweight tanks, was monitored by a dynamometer, and the object displacement was recorded by a specially designed displacement meter. The size and the shape of the testing objects are listed in Table 1. Correlation was attempted between the breakout force and the breakout time. The first approach was a theoretical analysis that attempted to correlate the various affecting parameters, such as dimensions and weight of the object, skin condition, embedment depth, water depth, soil properties, and rate of force application. Dimensional analysis showed that one of the possible correlations involved Reynolds number, Euler number, and Weber number. Results are presented in Reference 2.

Table 1. Description of Testing Objects

Object Number	Test Site	Shape	Dimensions (in.)	Weight in Air (lb)	Weight in Water (lb)	Remarks
1	San Francisco Gulf of Mexico	cube	74 x 74 x 74	35,500	20,000	Concrete
2	San Francisco Gulf of Mexico	parallelepiped	48 x 48 x 185	38,800	22,200	Concrete
3	San Francisco Gulf of Mexico	sphere	76.6 (diam)	23,500	14,500	Shell with concrete
4	San Francisco	cylinder	54 (diam) x 211.5	40,250	21,750	Shell with concrete
5	San Francisco	cone	length = 99.3, max diam = 75.5, min diam = 21	25,250	16,500	Shell with concrete
5A	San Francisco	ellipsoid	204 x 48	34,600	19,200	Shell with concrete
6	NCEL	cube	3 x 3 x 3	2.407	1.582*	Concrete
7	NCEL	parallelepiped	3 x 3 x 6	4.814	3.164*	Concrete
8	NCEL	sphere	2.5 (diam)	0.56	0.255*	Metal shell filled with sand

* These weights were taken in freshwater, the rest in seawater.

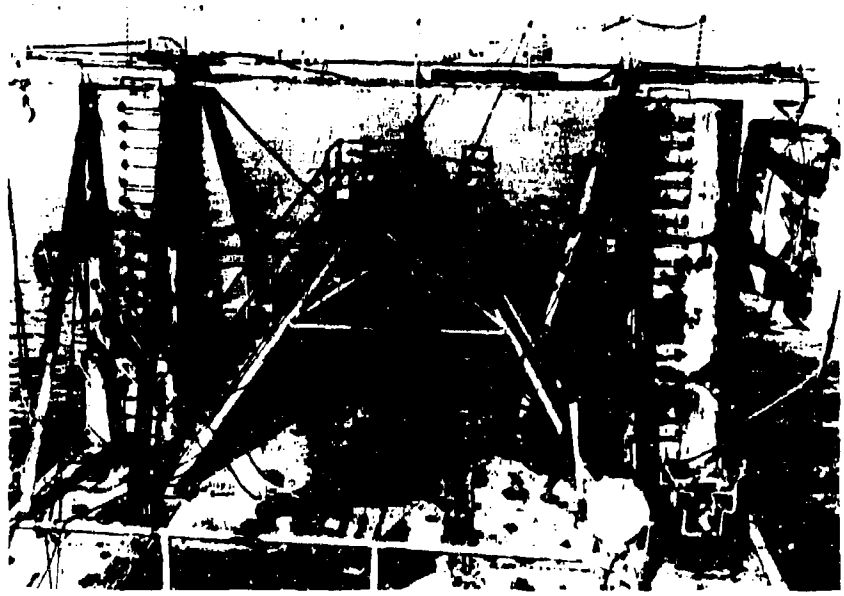

Figure 2. San Francisco field test arrangement.

Analytical Methods. Both soil mechanics and continuum mechanics have been considered as approaches to the breakout problems. Since the soil mechanics method seems to rely too heavily on empirical coefficients, the continuum mechanics method was selected to provide information independent of test results. This approach involves the following assumptions:

1. The soil is an isotropic and homogeneous continuum.
2. The soil has an elastic, perfectly plastic stress–strain property.
3. No stress creeping occurs.
4. The soil–object bond is much stronger than the strength of the soil.
5. The object is two-dimensional.

The continuum mechanics approach consists of solving boundary problems by the relaxation method. The boundary condition changes as the object is being pulled out. The maximum shear stress of the soil is calculated for each instantaneous boundary condition until its value exceeds certain failure

criteria. A computer program was written to calculate the breakout force and the total displacement of the object. The computer method is presented in Reference 2 in detail.

Work Done Outside NCEL

Breakout force research other than that conducted by NCEL includes the small-scale model study by R. C. DeHart and C. R. Ursell[3] of the Southwest Research Institute (SWRI), San Antonio, Texas, and some model studies by A. S. Vesić[4] of Duke University, Durham, North Carolina. The SWRI experiments were conducted in a 90-inch pressure vessel. The testing soils were sand and clay. Circular plates and a hemispheric shell were placed in the soil for a specific time before breakout tests. The results were considered preliminary and were not analyzed. The authors concluded that the breakout force depended upon object size, soil type, and in-situ time, and that the hydrostatic pressure had little effect on breakout.

APPROACHES

The large-scale field test is in general a most reliable tool for studying engineering problems. Since the test is performed in a natural environment, true field conditions are present. No assumption is necessary. Therefore, field tests were selected as the main tool to collect breakout force data. Nevertheless, the necessarily limited number of data points obtained may not be sufficient to cover all parametric variations. Two theoretical methods were therefore investigated to solve the breakout force problem: the applied mechanics method, which utilizes the dynamic system as a mathematic model, and the continuum mechanics method, which has a model of a static nature. They are discussed in the following paragraphs.

Applied Mechanics

The breakout problem may be treated as a simple dynamic system involving mass, damping, and resistance (Figure 3). The problem would then be approached by using a conventional dynamic equation of the following form:

$$My'' + Cy' + Ky = F(t) \qquad (1)$$

where* **M** = mass

C = damping coefficient

K = spring constant

F(t) = forcing function

y = displacement

y' = velocity, **dy/dt**

y'' = acceleration, $\mathbf{d^2y/dt^2}$

t = time

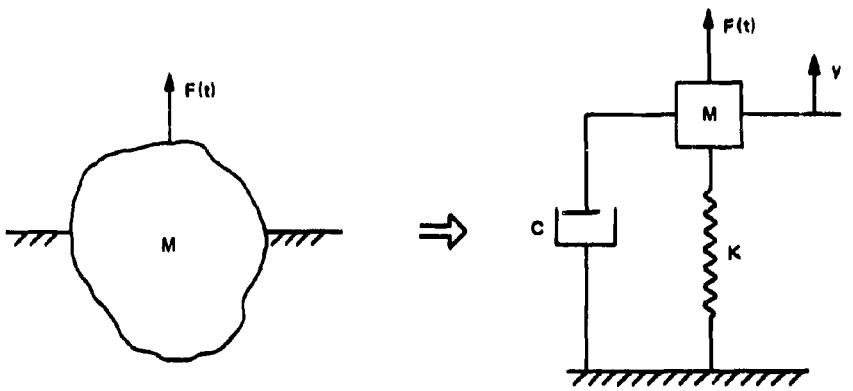

Figure 3. Analog of breakout system.

The mass **(M)** consists of the real mass **(m)** and virtual mass **(m')** of the object. The virtual mass depends upon the shape of the object, the densities of the fluids (ρ_w and ρ_s), and the displacement **(y)**. Thus, in mathematical terms, **M** = **M**(**y**, ρ_w, ρ_s, shape). The damping coefficient **(C)** is a function of water viscosity (μ_w), soil viscosity (μ_s), displacement **(y)**, velocity **(y')**, and object shape; thus, **C** = **C**(y, y', μ_w, μ_s, shape). The spring constant **(K)** is connected with the suction created under the object by lifting. It is assumed to depend upon the velocity **(y')**, soil permeability **(k)**, soil shear strength **(c)**, hydrostatic pressure **(p)**, object shape, and displacement **(y)**. We can write **K** = **K**(y, y', k, c, p, shape). The boundary conditions for the problem are:

* The reader is referred to the Nomenclature on the foldout page at the end of this report.

$$\text{at } t = 0, \qquad v = 0 \quad v' = 0 \quad v'' = 0$$

$$\text{at } t = T, \qquad y = y_b$$

where T is the breakout time and y_b is the displacement at breakout, which is an unknown itself.

The differential equation (Equation 1) is difficult to solve because (1) it is highly nonlinear, (2) y_b is unknown, hence the boundary condition is not complete, (3) the effects of object shape and soil properties are difficult to measure, and (4) it is not valid in two-phase fluids. Therefore, the applied mechanics approach is considered impractical to use to solve the breakout problem.

Continuum Mechanics

The second approach to this breakout problem is to treat the soil as a continuum and consider that the bond between the object and the soil is infinitely strong. This method also takes into account the plastic failure of the soil. However, since soil creep is excluded, breakout is not really treated as a time-dependent problem, but rather a finite-increment static problem. The procedure of solving the breakout problem involves first of all choosing an applied force increment starting from zero. For each force level the soil movement and maximum shear stress are calculated, with the aid of a computer facility, by a relaxation technique. The calculated stress is then compared with the elastic yield stress. The soil movement in the plastic stress region is calculated with plastic equations. For each load level, the local yield points are identified. As the load increases to a certain level, a complete failure line may be formed under the object. This force may be considered as the breakout force. Unfortunately, it is not possible to determine the breakout time using this method. Since this method simulates a series of static actions, an equilibrium condition for a load level can be reached only after a relatively long time period. Therefore, the resulting breakout force may be realized only by a very gradual extraction. This analytic method, although elegant, certainly does not simulate the actual operation, where the lifting load reaches its full level in a short period.

Without the support of an analytic solution, the field test data appeared to be very limited in quantity for making affirmative conclusions. Thus, more experimental data was needed. Since more field tests were not feasible due to a limited budget, a simple, small-scale model test program was developed to enrich the data bank.

BREAKOUT MECHANISM

Since the breakout problem involves many parameters (such as those discussed in the Applied Mechanics section), it is desirable to correlate only the important parameters and to eliminate the secondary ones. A thorough understanding of the mechanism of breakout motion will help determine the dominant variables and obtain qualitative relationships between them.

For instance, what happens when a lifting force is applied to an embedded object? What is holding the object down? To understand fully the breakout phenomenon the affecting factors should be identified and the influence of each of them upon the breakout force should be studied.

Mechanism of Object Breakout

Before discussing the breakout mechanism it would be beneficial to study the settlement of an object on marine sediment. Assume that the bottom soil is originally undisturbed. When an object is placed on the sediment, the weight of the object starts to drive itself into the soil. The maximum wall shear strength of the soil, the buoyancy force of the saturated soil, and the bottom bearing capacity combine into an upward-resistant force. Therefore, the depth of embedment depends upon the soil cohesion as well as upon the submerged weight, the maximum cross-sectional area, and the geometric shape of the object. The soil about the object may be considered slightly remolded, and the soil–object bond increases with the length of time the object has been embedded. The embedment may not stop even after a condition of apparent equilibrium is reached. The bearing pressure squeezes the water from the tiny pores between the soil particles and additional settlement results. This is a very slow process compared with the first stage of embedment.

When the object is first sunken into the saturated soil, remolding takes place where the object forces its way into the soil. The shear strength of the soil has been weakened, and the contact between object wall and soil is loose. But as time increases, the soil is forced back against the object by its static pressure, and the shear strength is also regained, at least in part, with time. Therefore, the longer an object is embedded in soil, the harder it is to break it loose from the bottom and the longer it takes.

During the period of settlement, there is hardly any assurance that the object will settle straight. In most cases the object will be tilted. Because the force equilibrium on the object is a relatively unstable one, any non-uniformity in soil resistance will produce an eccentricity on the resistance force, and an overturning moment results. This moment is only weakly

resisted by the side wall soil pressure. An inclination of the object will generally occur; spherical objects will simply rock about. Eventually the object will reach equilibrium.

Now let us apply a constant lifting force through the center of gravity of a settled object in equilibrium. This force, no matter how small, immediately destroys the equilibrium condition of the half-floating object, and a readjustment of the supporting forces takes place. The applied force first relieves the soil bearing pressure underneath the object. The object remains at its position after both bearing pressure and side friction force are counterbalanced. The balance of the lifting force will then produce an upward motion of the object, causing a loss of object buoyancy.

The displacement, velocity, and acceleration of every particle of the object are equal if the object is assumed rigid and not rotating. The upward motion of the object is likely to be resisted by some external forces, such as the stationary and viscous shear force of the surrounding soil and the soil tension resistance under the object. The stationary shear stress on the object wall is the friction force. But once the object begins to move, a velocity gradient is established between the object and the surrounding stagnate soil. Consequently, viscous shear stresses are developed in this zone. The thickness of the shear zone depends on the velocity of the object. The viscous shear stress is negligible for very slow breakout. Soil tension and shear resistances are transferred to the object through an interface adhesion bond and some times even through low-pressure pockets. The lifting force creates a pressure differential between the soil–water interface and the object–soil interface, causing a seepage flow towards the low-pressure area. The low-pressure condition is relieved as the water flows into the object–soil interface. But if the soil permeability is small, the vacuum will prevail for some time. Thus, even after the interface bond has failed locally, the high permeability of the soil permits the tensile stress transfer through a vacuum pocket between the soil and the object.

If the applied force continues to increase, a failure will eventually occur. This failure may be caused by any one or any combination of the following reasons: (1) soil shear stress failure, (2) adhesion force failure, (3) soil tension failure.

When the maximum shear stress in part of the soil becomes greater than the yield strength a local failure may occur. The local failure causes stress concentration in the vicinity of the failure point, and a crack line forms from the first failure spot. The yielding of the soil relieves some of the stress. This pattern of stress flow eventually creates a failure surface, and the object detaches completely from the soil. The whole process is a time-dependent phenomenon. It does not occur at once due to the plastic property of the soil.

A failure of the soil–object bond results in a quick breakout, especially for objects whose cross-sectional area becomes smaller with increasing depth below the mud line. This type of failure is likely if the top soil is sandy and the surface of the object is very smooth.

The third type of failure involves the tension strength of the soil. If the soil is homogeneous and isotropic, it is likely to fail in maximum shear strength first. The failure will occur earlier in tension if a sand layer exists in bottom clay. A failure will occur in a layer of soil of very weak cohesion, such as a saturated top layer of fine clay.

Mechanics of Object Breakout

If the force applied to the object during breakout is held constant with respect to time, the net breakout force is not constant. Once the object displacement starts, the depth of embedment and the soil buoyancy force decrease. Since the applied force is constant, the breakout force, which is the balance of the submerged weight of the object, must decrease.

The forces acting on an object placed at the water–soil interface are shown in Figure 4. The resultant force (**R**) may be expressed as

$$R = W - B_w - B_s - cA_s - \sigma A_x \qquad (2)$$

where W = dry weight of the object

B_w = water buoyancy force (lb)

B_s = soil buoyancy force (lb)

c = undrained shear strength of soil

σ = bearing strength of soil

A_s = side surface area of failure prism

A_x = base surface area of failure prism

The values of W and B_w are constant, whereas B_s varies with the embedded depth into the soil. This variation is dependent upon the object geometry. Both soil resistances cA_s and σA_x are depth and shape dependent.

Now let Equation 2 be illustrated in Figure 5. This sketch describes the force system at any displacement (y) of a right prism sinking vertically. Since the soil is saturated, the buoyancy force due to seawater is a constant. But the buoyancy of the soil is expressed as

$$B_s = (\gamma_s - \gamma) A_x y = C_1 y$$

where γ_s = specific weight of saturated soil

γ = specific weight of water

C_1 = constant

The B_s line in Figure 5 is therefore a straight line. The soil resistances (F_{rb} and F_{rs}) depend strongly upon the soil cohesion (c). They are expressed in general as

$$F_{rs} = \int_0^{A_s} c\, dA_s = (c/2) P y \qquad (3)$$

$$F_{rb} = \sigma A_x = 2 c A_x \qquad (4)$$

where P = perimeter of failure prism. But the cohesion increases with increasing depth, or approximately $c = C_2 y$. Therefore Equations 3 and 4 become

$$F_{rs} = C_2 P y^2 \qquad F_{rb} = 2 C_2 A_x y$$

The soil shear resistance increases with the square of the depth whereas the soil bearing resistance increases directly with the depth.

When the embedment reaches D the system is in equilibrium (R = 0). From Figure 5 it is easy to reason that the embedment is deeper if the wet weight of the object is heavier, the cross-sectional area is smaller, the specific weight of the soil is lighter, the soil cohesion is smaller, the cross-sectional area is more circular, or the cohesion gradient is smaller.

The cable attached to the object ready to be pulled out is generally arranged to allow the pulling force to align with the center of gravity of the object. The forces acting on the object at this time can be described by the expression

$$R = F_a - (W - B_w - B_s) - F_{rs} - F_{rt}$$

This force relationship at any embedment depth is illustrated in Figure 6.

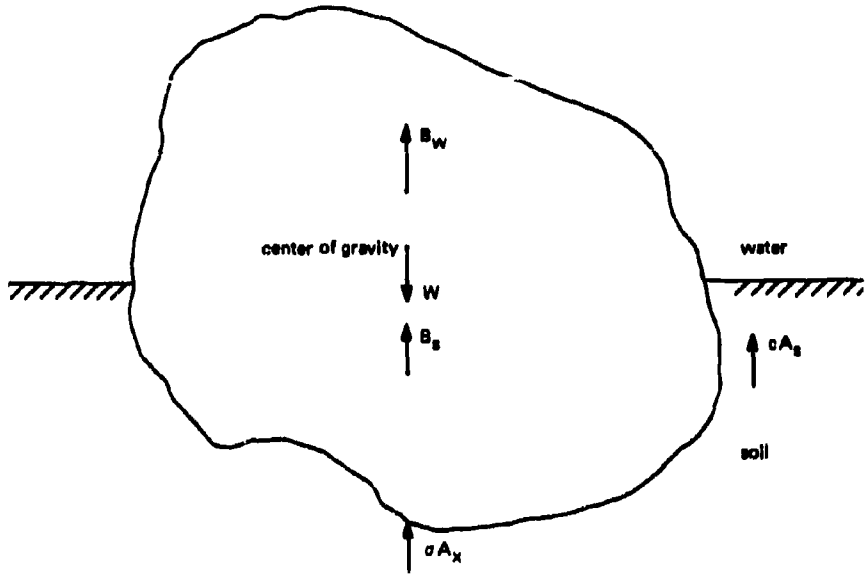

Figure 4. Forces acting on an object during breakout.

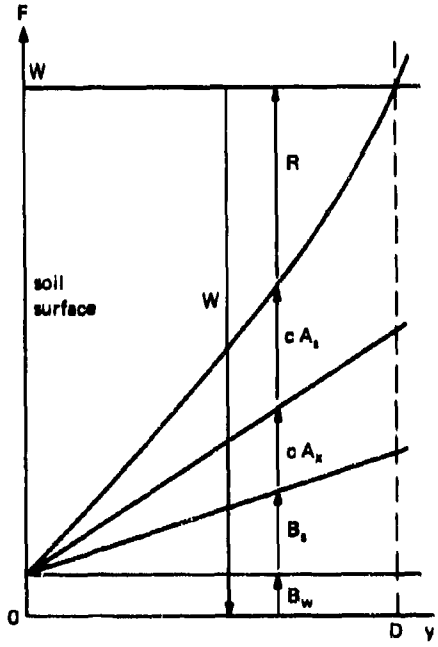

Figure 5. Force variations for a sinking right prism.

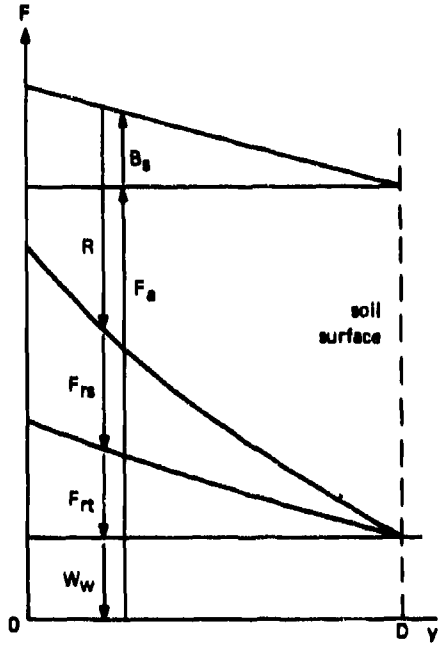

Figure 6. Force variations for a rising right prism.

The force variation diagram is also sketched for a vertical right prism. The resultant is the net upward force, which is the difference of load and resistance. The value of R could be negative; even then upward displacement will occur because of the local failure in the soil. The soil buoyancy (B_s) decreases as the embedment decreases. It varies directly with the embedment depth (D - y). The shear resistance (F_{rs}) again is proportional to the square of D - y, and the tension resistance of the soil is expressed as

$$F_{rt} = \sigma_t A_x = \frac{C}{2} A_x = \frac{C_2}{2} (D - y) A_x$$

where σ_t is the soil tension strength. Assuming the tension strength of the soil to be one-half of the cohesion, the tension resistance varies directly with D - y.

What is the relationship between D - y and R? The net upward force will increase with increasing D - y if the slope of the B_s line is smaller than the average slope of the resistance force curve.

For nonprism geometry the force diagram is much more complicated because the variation of the geometric properties of the object, such as the cross-sectional area and the shear surface area, are no longer linear functions of embedment (D - y). In this case it is very difficult to describe the variation of R with D - y. The B_s and F_r curves can be calculated from detailed information on the object geometry. It is generally very difficult to calculate tension resistance (F_{rt}) and the shear resistance (F_{rs}) for the curve-hulled object at various depth. For approximate values of F_{rt} and F_{rs} the curved bottom of the object may be transformed into a right prism of the same cross-sectional area but of slightly smaller depth. Engineering judgment must be exercised.

If R is a decreasing function, the breakout operation will require a larger extracting force or a longer breakout time. But for an increasing R during pullout, once the initial soil resistance is overcome, the breakout period will be relatively short.

Thus, the most important parameters affecting breakout time are the net extracting force (R) and the manner R varies with the displacement (y).

TEST PROCEDURES

Field Tests

A test site was selected off the Louisiana coast in the Gulf of Mexico. Very sticky clay soil was found in that area. Block 212 of the Louisiana oil lease area was surveyed and core-sampled before the actual tests. The results of the survey are reported in Appendix A.

The same test objects, cube, parallelepiped, and sphere, which were tested in San Francisco Bay were used again in the Gulf of Mexico. The tests were made in offshore ocean sediments under 100 feet of water. The test ship is shown in Figure 7. Two 8.4-ton salvage pontoons were assembled to provide variable vertical lift. The buoyancy of the pontoons was controlled by an air compressor. The lifting force was monitored through a line dynamometer, and the initial embedded depth of the test object was measured by divers. Details of the test procedure are presented in Appendix B.

A supplementary series of field tests was conducted on the 1,000-foot-deep ocean floor near Santa Cruz Island. Plates of various sizes were first forced into bottom mud 11 inches below the soil surface and were subsequently pulled out in less than 20 seconds. The plate displacement and the load on the plate were recorded on both oscillograms and magnetic tapes. Three square plates and seven circular plates were tested. The soil was fine clay. The test equipment is described in detail in Reference 5.

Laboratory Tests

The valid field test data were so limited that it was very difficult to interpret and correlate them. Additional data obtained from small-scale model tests augmented the field test results. Since the breakout process could be visualized with the model study, a clearer and more thorough understanding of the breakout phenomenon was gained. This understanding, in turn, provided the basis for a more logical selection of the correlating parameters.

The test equipment consisted of a container with soil, an extracting device, and a clock (Figure 8). The container was a 55-gallon used-oil drum with one end cut out. Inside the container was about 12 inches of mud, which was covered with 4 inches of freshwater. The metal drum was lined with heavy plastic sheets to prevent rusting. The extracting force was applied

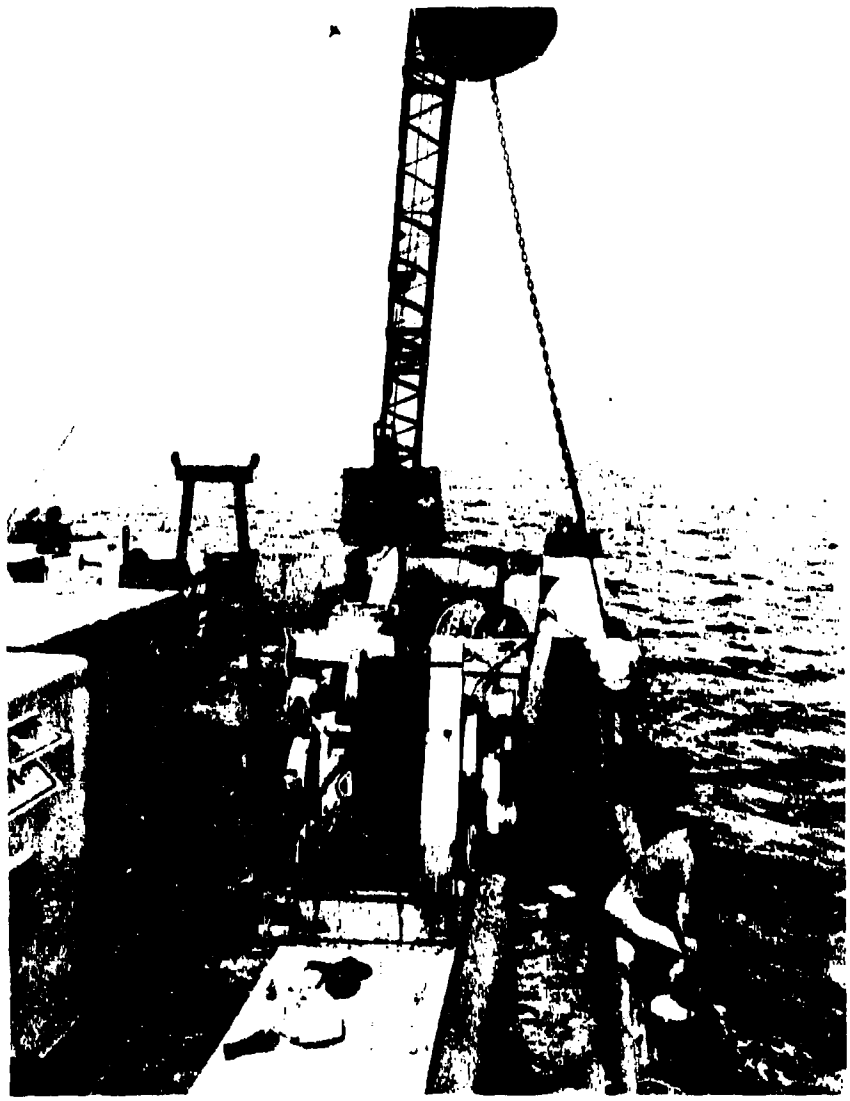

Figure 7. Field test ship at the Gulf test site.

and kept constant by a simple balance level. The total applied force on the object may be calculated from the hanging weights and the moment arms. The load application time or the breakout period was registered by an electric clock with a mercury switch. At the time of pullout, the test object would travel some distance upward to reach a new balance, causing the level to tilt. This action triggered the switch and stopped the clock.

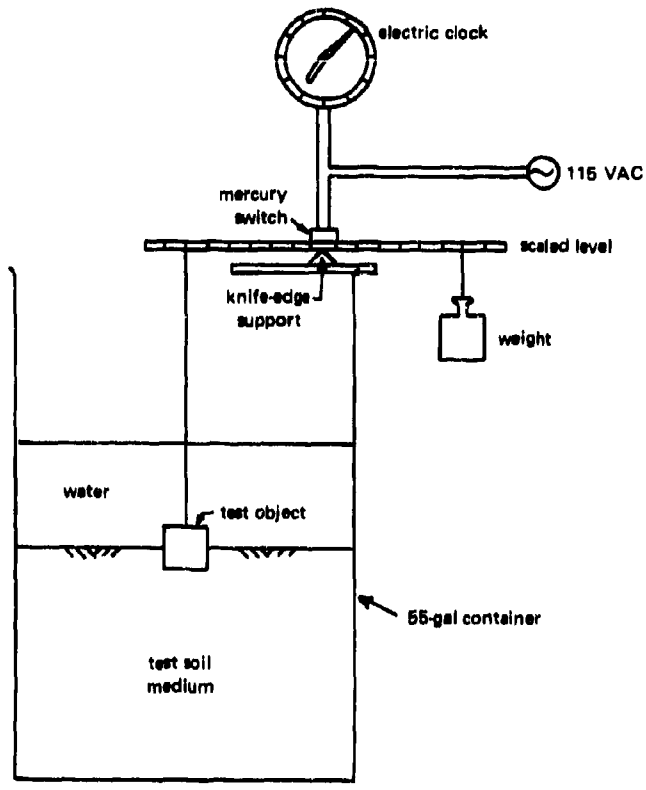

Figure 8. Setup for model breakout tests.

First, the test soil was disturbed to remove any irregularity on the soil surface. After sufficient time for the soil to settle and regain its strength, the test object was very carefully placed on top of the soil near the center of the drum. The test object was allowed to settle for a specified time before a load was applied for breakout. The total settlement of the object was measured with a specially designed ruler. At the beginning of the pullout, weights were hung at proper distances from the pivot point of the level to produce a desired pullout force.

The test soils were obtained from the nearby Point Mugu Lagoon and from the Ocean Bottom Simulating Facility at Seal Beach, California. The Seal Beach soil is coarser than the Mugu soil (see Appendix A).

DATA REDUCTION

It is general practice to make a dimensional analysis before trying to derive an empirical formula. The purpose of such an analysis is to reduce the number of varying parameters to a minimum. The variables that affect breakout may be listed as follows:

1. Specified breakout time (**T**).
2. Applied force: magnitude (F_a), eccentricity (**e**), rate of application (dF_a/dt).
3. Object geometry: maximum cross-sectional area under soil (A_m) embedded depth (**D**), shape, surface roughness (ϵ), mass (**m**).
4. Soil properties: density (ρ_s), viscosity (μ_s), shear strength (**c**), tension strength (σ_t), permeability (**k**), object settlement time (T_{in}), stress creeping characteristics, mean grain size (δ).
5. Water properties: density (ρ_w), viscosity (μ_w), depth (**h**).

The time required for pullout depends on the amount of force applied to an object, the rate of application, and the location of the application. The applied force must be larger than the submerged weight of the object in seawater to achieve breakout. But forces slightly larger than the submerged weight of the object partially embedded in mud may cause an initial upward displacement that is not enough for complete pullout. As the force increases, the time for breakout decreases to almost zero. At this time, the breakout force is the maximum force required. If the force is gradually applied, then the rate of the application would affect the breakout time. A quick breakout may result from a rapid application of force. If the force is applied at an eccentricity to the centroid, a rotating moment results. The moment would tend to create a nonuniform distribution of the bearing pressure under the object and to accelerate local failure. Thus, with an eccentric uplifting force the breakout action is speeded up. The lifting force required would then be smaller.

Although settlement and breakout are essentially opposites, parameters affecting the one are likely to affect the other. For instance, the longer the settlement time of the object, the longer the time required for breakout. The effect of embedded depth on the breakout is very hard to estimate. It is a function of object geometry, object mass, soil density, soil cohesion, soil bearing force, and settlement time. For the same object and settlement time, deeper embedment suggests a weak soil. Breakout time is directly proportional to embedded depth, but it is also directly proportional to soil cohesion. A deep initial embedment may or may not suggest a large breakout force because the soil cohesion must be weak.

The geometric shape of the object affects the breakout too. The mass of the object is related to the embedded depth, which in turn is related to the breakout force. Large mass tends to slow down rapid breakout but has little effect on slow movements.

Fine soil, like clay, develops a high adhesive strength on rough surfaces. Smooth surfaces have less contact area with soil particles and lead to an earlier breakout.

If the embedded portion of the object presents sharp-angled edges, local interface bond failure or soil shear failure occurs much earlier than it does for smooth-surfaced objects. The failure surface for the sharp-angled object is also larger than that of a smooth object. There is much less side friction for a spherical or a streamlined body than there is for a rectangular parallelepiped. Therefore, it is expected that the time required for spherical objects to break out is shorter than that for cubic or parallelepiped objects of equivalent size.

The width-to-length ratio of a parallelepiped seems to affect the breakout time, because of the nonuniform distribution of the bearing stress under the object. It is expected that the tension stress distribution under the object during breakout is also nonuniform. Local failure occurs earlier in soil for objects having nonuniform stress distribution. Therefore, it is expected that a long, narrow parallelepiped is easier to break out than a cube having the same horizontal cross-sectional area and weight.

The object surface area under the soil is directly proportional to the resistance produced by either soil adhesion or cohesion. A curved-surface object such as a sphere usually has less surface area than a comparable sharp-angled object such as a cube. However, the difference in surface area is expected to be relatively small.

Soil properties are major factors that control pullout. It is agreed that breakout is no problem in sand. First, sand has a large grain size and hence little adhesion strength. Second, the permeability of sand is so large that a vacuum pocket cannot exist. Last, the cohesion of sand is small. Therefore, the affecting parameters are identified as the soil grain size, soil permeability, and soil cohesion.

Another parameter is soil viscosity. This factor affects breakout most when the speed of the object movement is appreciable. The transient time of the breakout depends upon soil viscous damping. Unfortunately the viscosity of saturated soil is very difficult to determine. It is also difficult to estimate viscous damping in a two-phase medium such as soil.

Soil density also affects breakout, but the range of its variation is small enough to be neglected.

Hydrostatic pressure at the soil surface may play an important role in breakout. It may increase seepage flow and reduce soil resistance.

With the above considerations, the breakout phenomenon may be described by the expression

$$f\left(F_s, T, e, \frac{dF}{dt}, A_m, D, \epsilon, m, \text{shape}, \rho_s, \mu_s, c, \sigma_t, k, T_{in}, \text{creeping}, \delta, \rho_w, \mu_w, h\right) = 0$$

It is evident that a dimensional analysis cannot be made with so many affecting parameters. In order to simplify the relationship, less important parameters may be eliminated and others combined into new parameters.

Seawater has a fairly constant density and viscosity most of the time. The parameters ρ_w and μ_w would have very little effect on breakout. The permeability (k) of the ocean bottom soil is very high in general, and the grain size (δ) is small. Thus the range of variation for k and δ is small and may be neglected too. The possibility of a sand ocean bottom is of no concern since such a condition would not create a serious breakout problem.

Accordingly, the soil resistance to breakout may be expressed as

$$F_r = F_r(A_m, D, c, \sigma_t, \text{shape})$$

the soil buoyancy force is written as

$$B_s = B_s(\rho_s, A_m, D, \text{shape})$$

The net breakout force is

$$F = F(F_s, m, B_s, \rho_w)$$

and the dynamic damping may be written as

$$D' = D'(\mu_s, k, \text{creeping})$$

With the above parameter grouping and elimination, the breakout may now be looked at as

$$f\left(T, F, F_r, T_{in}, D', e, \frac{dF}{dt}, \epsilon, m, h\right) = 0$$

Now if we further assume that the parameters D', e, ϵ, m, and h are kept constant during the experiment and that the effect of the variation in buoyancy is small, then the breakout may be expressed as simply

$$\frac{F}{F_r} = f\left(\frac{T}{T_{in}}\right)$$

All data are reduced into the form of F/F_r versus T/T_{in}. During the field tests it was not practical to apply abruptly a constant load of about 20,000 pounds. Occasionally the load level is increased in the middle of a test to speed up pullout. Thus, the applied loads were not kept constant at all times. To facilitate the correlation calculation, an effective time was calculated from the force history curve:

$$T_e = \frac{\int_0^T F_a \, dt}{(F_a)_{max}}$$

The effective time is further illustrated in Figure 9. This is equivalent to the time expended if the force $(F_a)_{max}$ were applied at the beginning of the test. The net breakout force is calculated by the equation

$$F = F_a - W_w + B_s$$

where $B_s = (\rho_s - \rho_w) g V_s$

V_s = volume of soil displaced by object

W_w = weight of object in water

The calculation of soil resistance is based on the assumption that the object–soil adhesion is stronger than the soil cohesion. For a prism, the failure is assumed to occur in the soil near the object rather than along the wall of the object.

An accurate evaluation of the soil resistance under a nonprismatic object involves a complicated evaluation of integrals. The resistance is expressed as

$$F_r = \int_0^A (c \sin\phi + \sigma_t \cos\phi) \, dA$$

where ϕ is the inclination angle of the element dA. The limit A means to integrate over the object's embedded surface. The calculation of F_r is very time consuming.

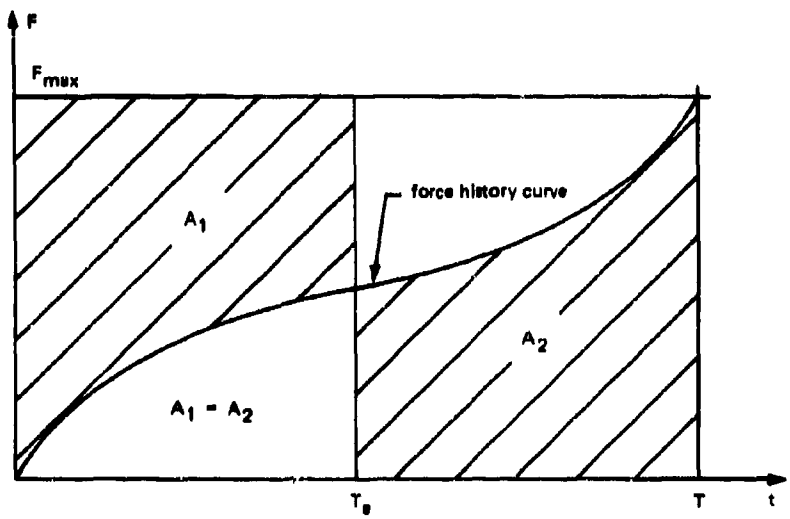

Figure 9. Definition of effective breakout time.

To simplify the calculation, a shear prism is assumed to exist with the base area (A_x) equal to the maximum horizontal cross-sectional area of the embedded portion of the object, and the prism height is assumed to be one-half of the embedded depth.

The cohesion $\bar{c}$ is the average shear strength taken over the embedded depth of the shear prism and is assumed to be one-half of the shear value at the bottom of the shear prism. The tension strength of the soil is taken as one-half of the cohesion for saturated fine clay. Thus, the tension strength (σ_t) is equal to the average cohesion ($\bar{c}$). The resistance of the soil to breakout is equal to the product of the average cohesion and the surface area of an imaginary shear cylinder or prism. The equation used in data reduction is is

$$F_r = \bar{c} A_s + \sigma_t A_x \qquad (5)$$

But $\bar{c} = \sigma_t$. Therefore,

$$F_r = \bar{c}(A_s + A_x)$$

The soil cohesion profiles were obtained at selected coring sites. It is not practical to measure the cohesion profile at each individual test site. The average cohesion at each test site is best estimated by interpolation of the

existing cohesion profile. The measured cohesion profiles for San Francisco and the Gulf of Mexico are shown in Figures 10 and 11, respectively, and the locations of the coring and test sites are shown in Figures 12 and 13. The cohesion profiles for the laboratory test tanks are presented in Figure 14.

An examination of the data obtained in San Francisco Bay shows that the spacings between test sites are too small. Several test sites have been used repeatedly, as shown in Figure 12. Thus, the latter tests are actually performed on remolded soil. Corrections were made on the average soil cohesion by assuming that the remolded soil cohesion is only one-half of the cohesion strength of the undisturbed soil.

Because of the large number of data points and the press of time, a Fortran II computer program was prepared to make rapid calculations and plottings. It proved to be an effective tool for selecting by trial and error the most suitable correlation.

RESULTS AND DISCUSSION

Presentation of Results

All the experimental results are presented in a dimensionless plot in the form of a correlation, as shown in Figure 15. With such a generalization, these data may be used for a wide range of object sizes and soil conditions. The vertical coordinate F/F_r is the ratio of the net breakout force to the estimated soil resistance. This ratio represents the degree of loading on the soil. The horizontal coordinate T/T_{in} is simply a time scale for the measurement of breakout time. The object settlement time (T_{in}) is also a control parameter of the breakout phenomenon. If the soil is looked upon as a rheological model, then there must be a relationship between the degree of loading and the time elapsed.

The data in Figure 15 consist of results obtained in all three separate experimental studies. All the experimental data are also given in Table 2. The results of the San Francisco Bay field tests have been published in a previous NCEL report by Muga,[2] but were presented in a different correlation. They are included here to test the effectiveness of the Liu correlation method. Gulf data and model study data are new data. The Gulf soil has definitely different properties from the Bay soil, but the objects tested were identical in both field tests. The model study used objects having length scales 25 to 30 times smaller than those used in the field tests. In addition the test soil was remolded in the model study. With all these differences between the three experimental studies, the data points seem to cluster together very

well. Thus, the effect of soil properties and object shape and size has been at least partially taken into consideration by this form of correlation. The convergence of the data also proves that generalization by nondimensionalizing the breakout force and the breakout time is valid, at least for the variations in soil cohesion, object size, and object shape present in these studies.

The Gulf of Mexico field test results are presented in Figure 16. The scatter of the data points is large, but the general trend is clear. The effect of object geometry on breakout is not apparent here.

The soil surface conditions seemed to affect the test results to a great extent. Shell fragment layers were found at the San Francisco Bay site. The presence of coarse materials in fine clay tends to decrease the bonding strength between the object and the soil. This effect is more serious for spherical and horizontal circular cylindrical objects. Objects having a vertical contact surface would be affected only slightly, depending upon the area of vertical shear. Therefore, the San Francisco Bay data show smaller than expected breakout forces for the sphere and the circular cylinder. Even the data for the cube and the prism are slightly smaller than expected because of the reduction of bonding strength at the bases of the objects. There is no such problem in the Gulf test site. However, for small-scale model tests in laboratory tanks, after a repeated stirring up and settling of the test soil, natural gradation occurs. A layer of extra fine poorly cemented clay particles covers the test site. Since the bond between particles is small, soil cohesion reduces to very small values. The estimated soil resistance again becomes too large and the data points fall too low on the breakout correlation graph. Again this affects the sphere pullout tests more than the cube tests. If the invalid data points are eliminated, the correlation is replotted, as shown in Figure 17.

The test data are for objects embedded only for a short time in the sea floor, when only the first stage of the settlement has been completed.

Table 2. Experimental Data

Run No.*	Object**	Embedment (in.)	In-Situ Time, T_{in} (hr, min)	Applied Force (lb)	Breakout Time, T (min)	Cohesion (psf)	Breakout Force, F (lb)	Soil Resistance, F_r (lb)	Force Ratio, F/F_r	Time Ratio, T/T_{in}
014	3	36.00	17, 0.0	16,000	317.0	116.00	3,792	7,188	0.5276	0.3107
024	4	27.00	102, 0.0	24,200	41.0	43.00	47,018	49,451	0.9508	0.0066
027	3	34.00	36, 0.0	19,600	46.0	120.00	7,196	7,201	0.9994	0.0212
028	3	26.00	12, 0.0	18,000	37.0	116.00	4,847	5,849	0.8287	0.0513
029	3	60.00	70, 0.0	15,350	483.0	79.00	5,281	7,921	0.6667	0.1150
030	3	36.00	13, 0.0	15,500	467.0	115.00	3,292	7,126	0.4620	0.5987
033	4	30.00	21, 0.0	21,700	205.0	86.00	54,422	119,323	0.4560	0.1626
034	1	48.00	19, 0.0	29,000	89.0	47.00	14,628	6,424	2.2768	0.0780
035	2	20.00	26, 0.0	28,600	44.0	76.00	10,202	9,605	1.0621	0.0282
036	2	18.00	18, 0.0	30,700	165.0	72.00	11,922	8,634	1.3808	0.1527
037	2	20.00	16, 0.0	27,700	119.0	65.00	9,302	8,215	1.1323	0.1239
038	1	36.00	68, 0.0	30,300	64.0	79.00	14,521	8,850	1.6407	0.0156
042	1	54.00	93, 0.0	27,200	147.0	72.00	13,531	10,730	1.2611	0.0263
043	1	58.00	96, 0.0	25,300	112.0	65.00	12,100	10,221	1.1838	0.0194
046	2	12.00	240, 0.0	32,200	118.0	37.00	12,281	3,718	3.3028	0.0081
048	1	44.00	162, 0.0	23,500	62.0	61.00	8,659	7,836	1.1049	0.0063
049	2	30.00	115, 0.0	25,600	75.0	25.00	9,104	3,968	2.2939	0.0108
050	1	40.00	44, 0.0	22,000	399.0	58.00	6,690	6,974	0.9592	0.1511
051	2	27.00	42, 0.0	24,600	46.0	22.00	7,533	3,278	2.2976	0.0182
052	4	28.00	24, 0.0	25,000	167.0	29.00	51,120	35,649	1.4339	0.1159
053	2	34.00	43, 0.0	30,700	254.0	87.00	14,964	14,937	1.0018	0.0984
054	4	30.00	42, 0.0	26,000	34.0	58.00	58,722	80,473	0.7297	0.0134
103	1	22.00	21, 24.0	36,000	6.5	52.00	18,021	4,328	4.1630	0.0050
108	3	30.50	11, 33.0	18,000	3.7	70.00	4,879	3,931	1.2412	0.0054
109	3	32.50	22, 37.0	22,000	230.0	72.00	9,029	4,206	2.1465	0.1694
110	3	27.00	14, 10.0	22,000	3.7	62.00	8,626	3,210	2.6871	0.0043
113	3	12.00	68, 42.0	17,000	128.5	32.00	2,760	862	3.2021	0.0311
114	3	17.00	21, 48.0	17,500	8.5	44.00	3,497	1,597	2.1890	0.0064
115	3	26.00	2, 6.0	16,500	152.0	62.00	3,056	3,126	0.9775	1.2063
116	3	28.00	62, 30.0	21,000	5.2	66.00	7,697	3,503	2.1970	0.0013
117	3	24.00	4, 0.0	16,600	7.2	60.00	3,020	2,855	1.0575	0.0300
118	3	25.00	41, 21.0	21,300	15.0	63.00	7,787	3,089	2.5209	0.0060
120	3	29.00	12, 9.0	18,800	18.0	68.00	5,569	3,695	1.5070	0.0246
122	3	19.00	16, 51.0	20,800	4.5	50.00	6,908	1,987	3.4757	0.0044
124	3	31.00	11, 0.0	17,500	105.2	70.00	4,416	3,972	1.1120	0.1593
125	2	7.50	600, 0.0	24,000	311.0	22.00	2,917	1,890	1.5432	0.0086
126	2	4.00	13, 52.0	23,200	100.0	14.00	1,596	1,044	1.5280	0.1201
127	1	12.00	47, 47.0	22,000	132.0	32.00	3,102	2,006	1.5465	0.0460
128	2	10.50	46, 52.0	26,000	6.0	30.00	5,364	2,869	1.8696	0.0021

Table 2. Continued

Run No.*	Object**	Embedment (in.)	In-Situ Time, T_{in} (hr, min)	Applied Force (lb)	Breakout Time, T (min)	Cohesion (psf)	Breakout Force, F (lb)	Soil Resistance, F_r (lb)	Force Ratio, F/F_r	Time Ratio, T/T_{in}
301	6	2.20	23, 50.0	1.8980	227.0	1.80	0.6414	0.4425	1.4495	0.1587
314	7	5.50	18, 41.0	5.0000	5.0	4.10	2.6495	2.1354	1.2407	0.0044
316	6	3.00	4, 5.0	1.8100	7.4	2.80	0.6717	0.8749	0.7677	0.0302
317	8	1.30	4, 55.0	0.4000	3.0	1.40	0.1848	0.0992	1.8626	0.0101
318	6	3.00	21, 53.0	2.3000	1,360.0	2.80	1.1617	0.8749	1.3277	1.0357
319	8	1.90	21, 42.0	0.3500	87.0	1.70	0.1487	0.1761	0.8446	0.0668
320	8	1.70	17, 0.0	0.3000	127.0	1.60	0.0946	0.1483	0.6381	0.1245
321	8	1.50	20, 36.0	0.3407	13.0	1.50	0.1306	0.1227	1.0645	0.0105
322	6	3.00	17, 7.0	2.1800	38.0	2.20	1.0417	0.6874	1.5152	0.0370
324	8	1.50	3, 45.0	0.3188	124.0	1.50	0.1087	0.1227	0.8861	0.5511
326	8	1.50	64, 35.0	0.3188	1,443.0	1.50	0.1087	0.1227	0.8861	0.3723
327	8	1.20	5, 9.0	0.2750	2.0	1.30	0.0573	0.0867	0.6605	0.0064
328	8	1.20	19, 20.0	0.2656	10.0	1.30	0.0479	0.0867	0.5522	0.0086
329	8	1.10	24, 14.0	0.2578	51.0	1.30	0.0375	0.0826	0.4545	0.0350
330	8	1.00	5, 36.0	0.2609	7.5	1.30	0.0381	0.0779	0.4894	0.0223
331	8	0.85	17, 11.0	0.2578	15.0	1.20	0.0314	0.0645	0.4879	0.0145
332	8	0.80	0, 18.0	0.2578	3.5	1.20	0.0303	0.0617	0.4912	0.1944
333	8	0.70	1, 5.0	0.2578	2.3	1.20	0.0281	0.0558	0.5044	0.0353
334	8	0.85	2, 0.0	0.2578	1.4	1.20	0.0314	0.0645	0.4879	0.0116
338	6	1.00	0, 17.0	2.4000	0.5	1.30	0.9659	0.1895	5.0949	0.0294
339	6	1.30	0, 15.3	2.0000	4.7	1.40	0.6102	0.2391	2.5517	0.3071
340	6	1.50	0, 15.5	2.0000	116.5	1.50	0.6398	0.2812	2.2751	7.5161
343	6	1.00	0, 20.0	1.8000	6.7	1.30	0.3659	0.1895	1.9301	0.3350
344	6	1.25	0, 14.5	1.8000	22.3	1.35	0.4028	0.2250	1.7906	1.5379
345	8	0.95	67, 7.5	0.2578	9.5	1.25	0.0338	0.0725	0.4667	0.0023
402	8	2.20	24, 2.0	0.2960	136.0	1.80	0.1190	0.2159	0.5510	0.0943
425	6	3.25	65, 41.0	2.7040	11,858.7	2.90	1.7652	0.9666	1.8260	3.0090
446	7	5.60	18, 11.0	5.0000	1,168.0	4.20	2.9443	2.2224	1.3247	1.0705

* The first digit of the run number indicates the test phase: 0 = San Francisco Bay field tests, 1 = Gulf of Mexico field tests, 3 or 4 = Laboratory model tests.

** The object number is defined in Table 1. Data for objects 5 and 5a are not given because of their poor quality.

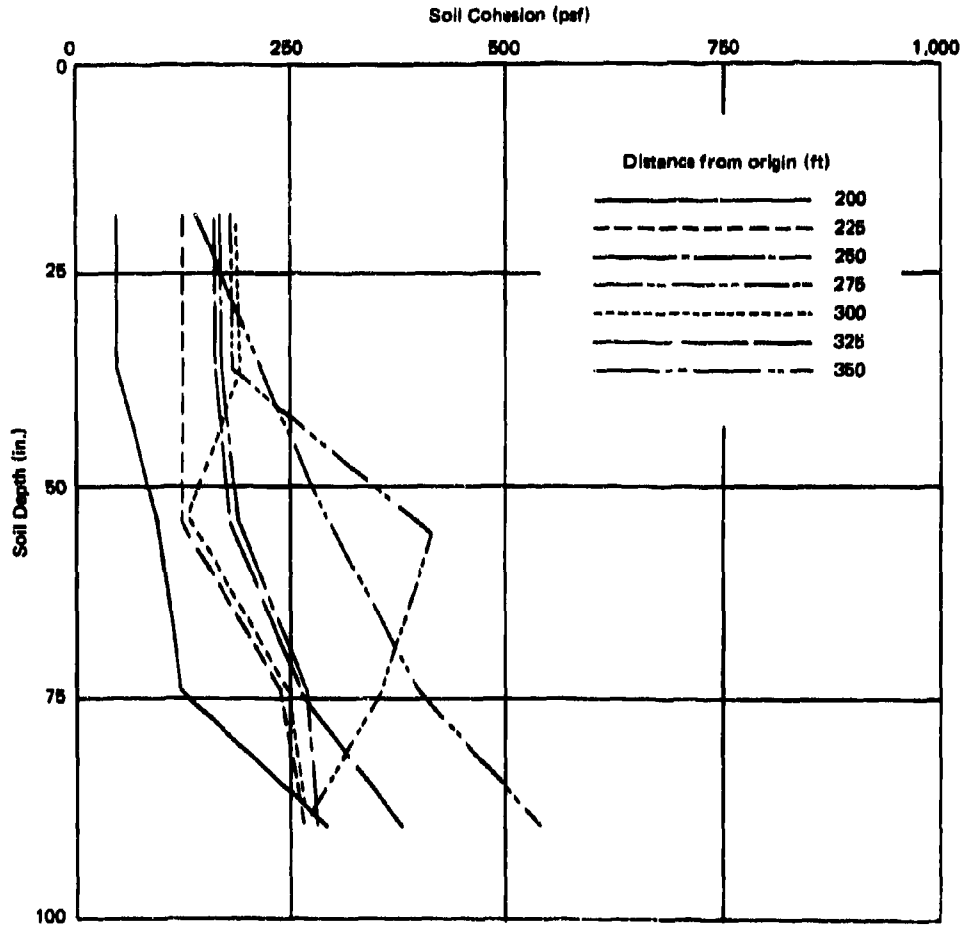

(a) Bearing 93.0°.

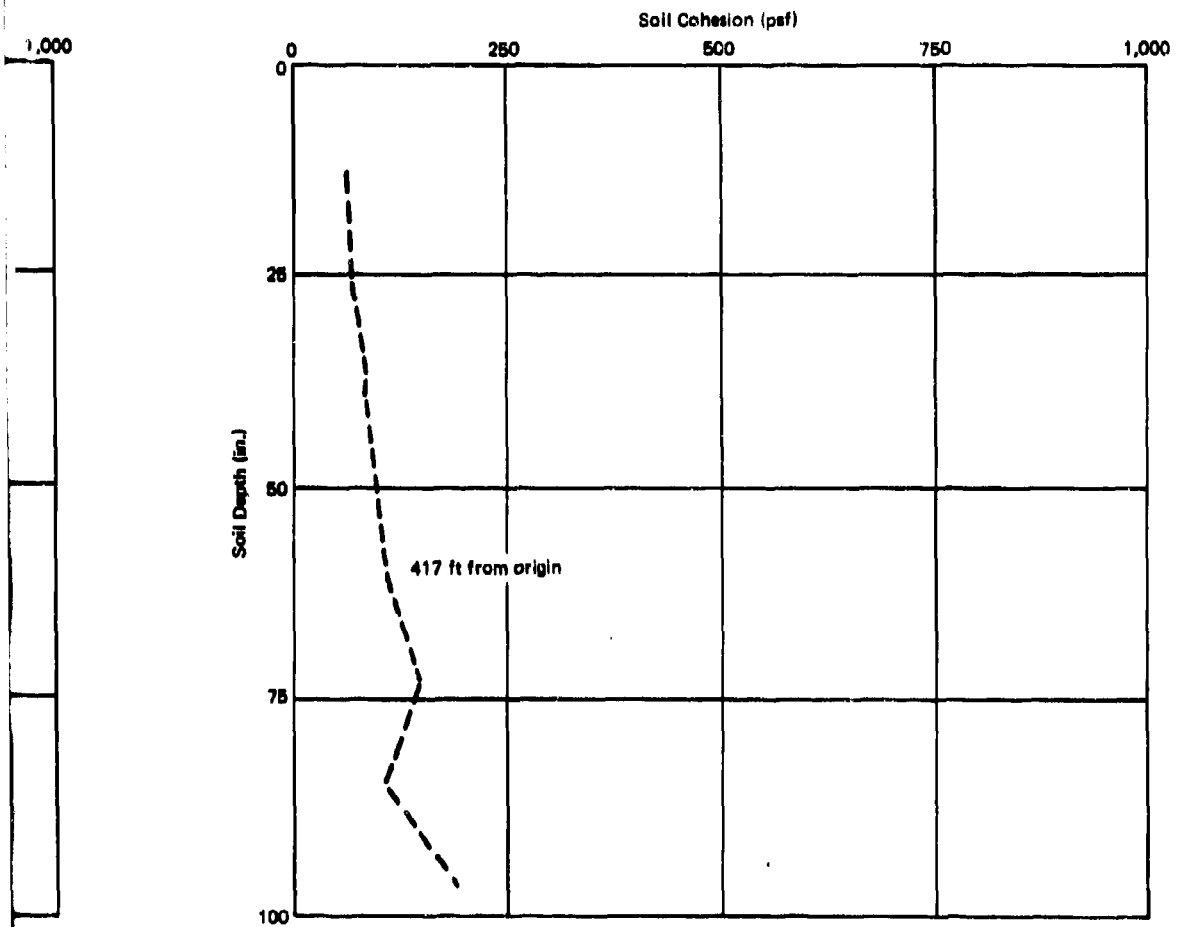

(b) Bearing 91.1°.

Figure 10. Soil vane shear strength profiles for San Francisco Bay test sites.

12

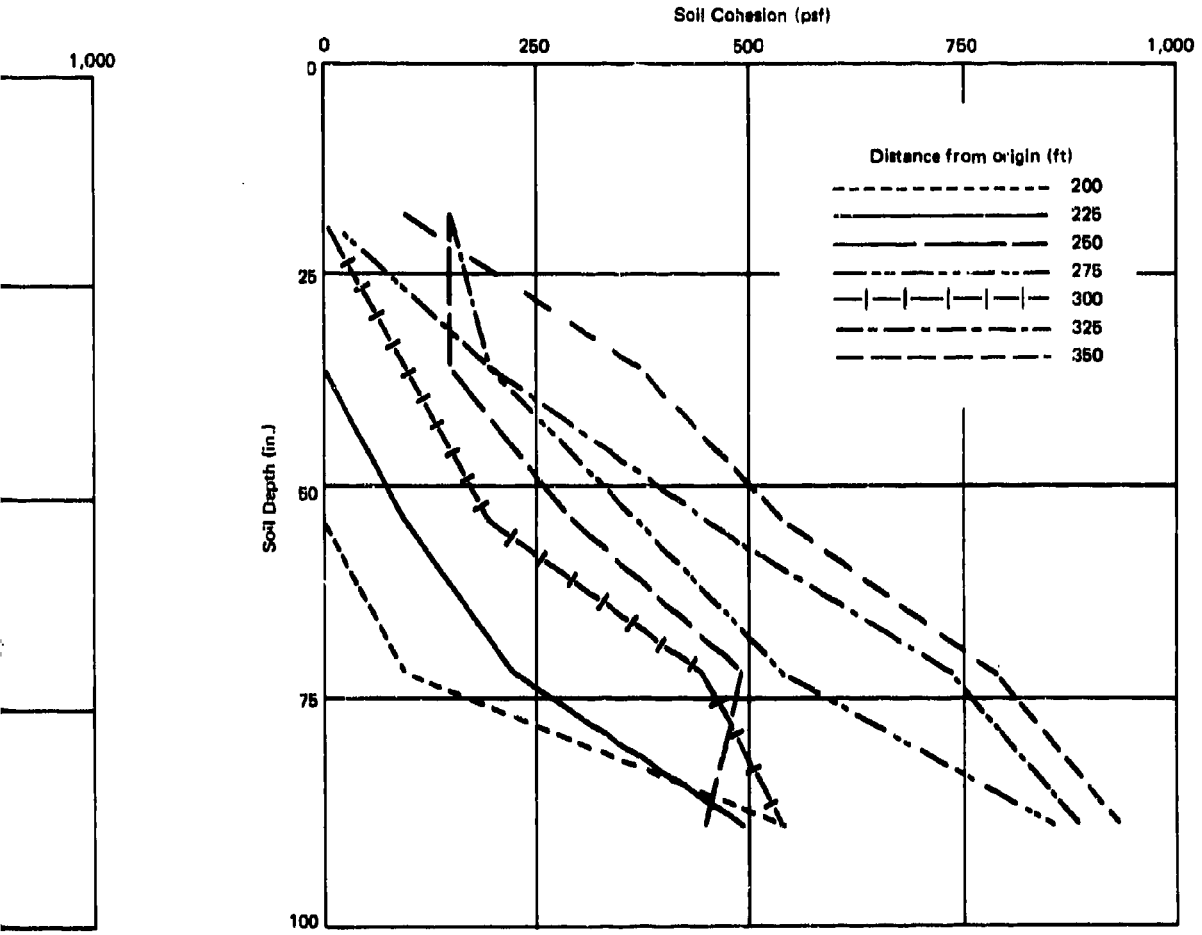
Soil Cohesion (psf)
0
250
500
750
1,000
Soil Depth (in.)
0
25
50
75
100
Distance from origin (ft)
200
225
250
275
300
325
350

(c) Bearing 87°.

THIS

PAGE

IS

MISSING

IN

ORIGINAL

DOCUMENT

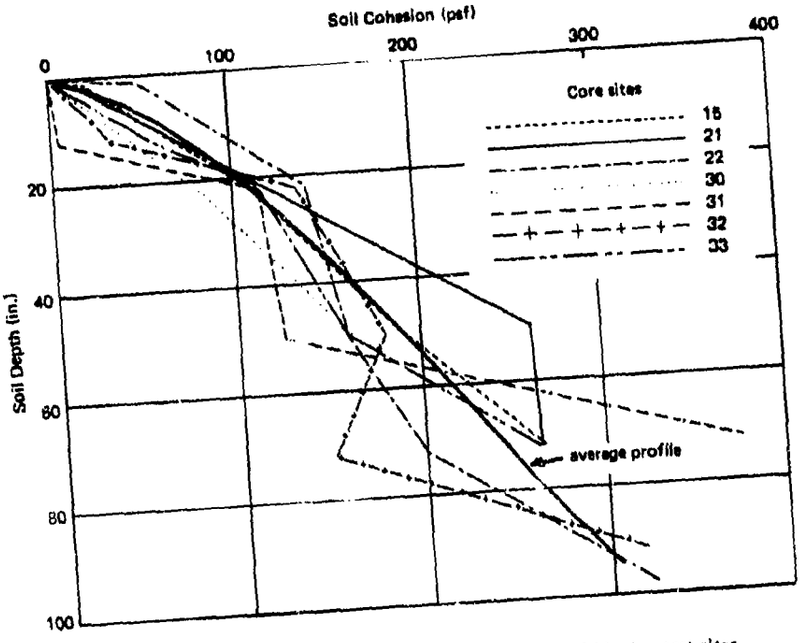

Figure 11. Soil vane shear strength profiles for Gulf of Mexico test sites.

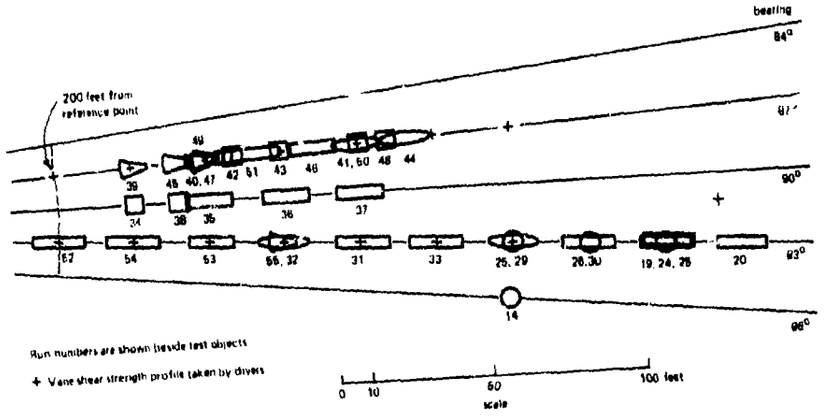

Figure 12. Location map for San Francisco Bay test sites.

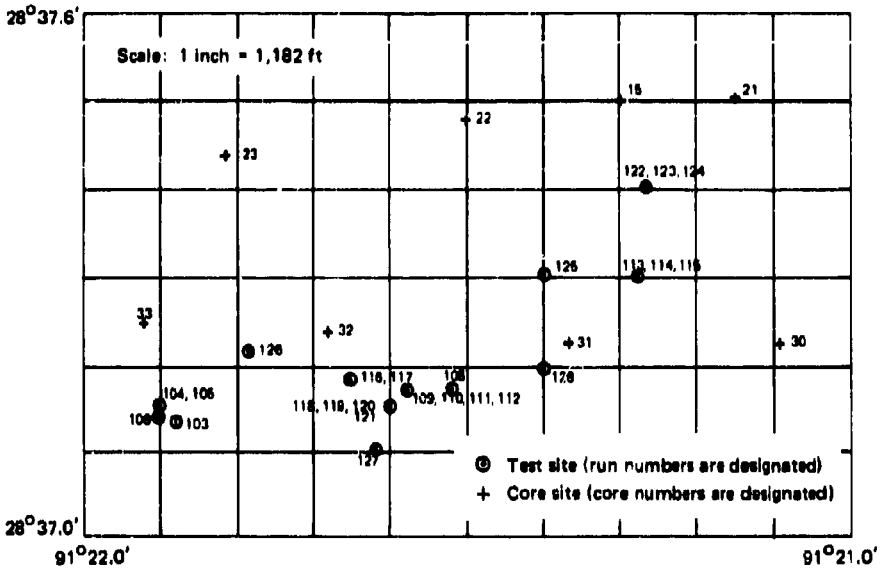

Figure 13. Location map for Gulf of Mexico test sites and nearby coring sites.

Method of Correlation

Three groups of data are represented to test the method of correlation. The San Francisco Bay data were first correlated by Muga in the following empirical formula (from Reference 2):

$$F = 0.20 A_m q_d e^{-0.00540(T - 260)}$$

where F = breakout force (lb)

A_m = horizontal projection of the maximum contact area (in.^{2})

q_d = average supporting pressure provided by the soil to maintain the embedded object in static equilibrium (psi)

T = time allowed for breakout (min)

The scattering of the data is great, and there are not enough data points to cover the whole range of the curve. In addition, the correlation lacks physical meaning. The embedment, which is an important parameter, is not included in the correlation.

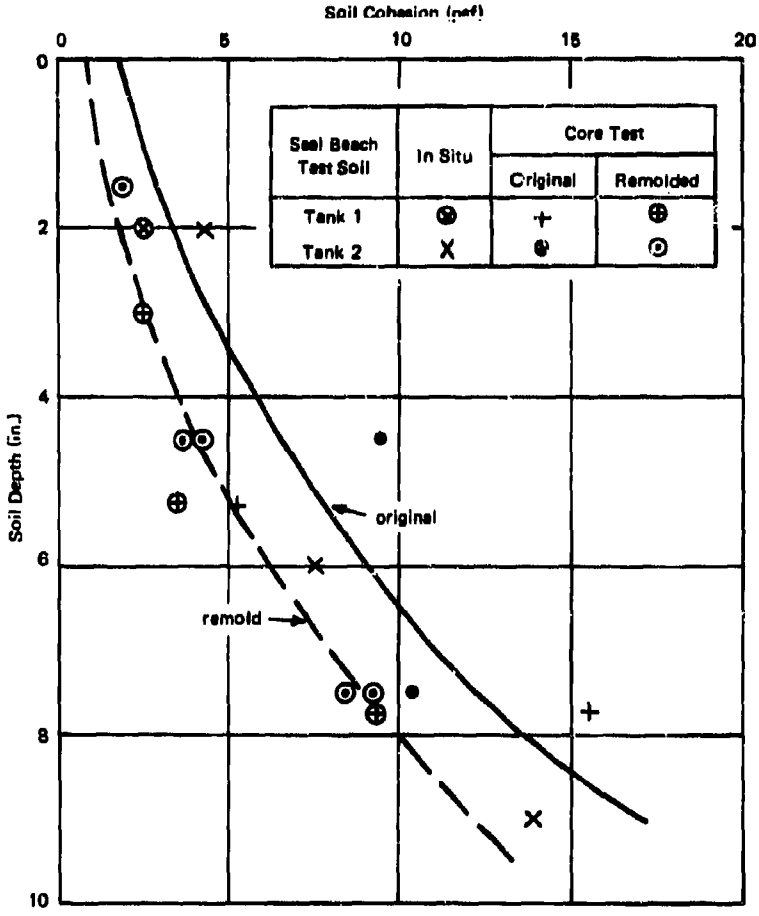

Figure 14. Cohesion profile of model study soils.

This correlation was later improved by including the displacement (y) and the shape factor (C_s). Good correlations were obtained for both the San Francisco and Gulf data by assigning proper values of C_s to take care of the geometry difference, as shown in Figure 18. However, Muga's correlation cannot be generalized to include conditions other than the size range of the test objects, namely, in the 20,000-pound range, and in the soil depth range of about 5 feet. The small-scale model data disagree with the field test data to a great extent when plotted in the form of Muga's correlation.

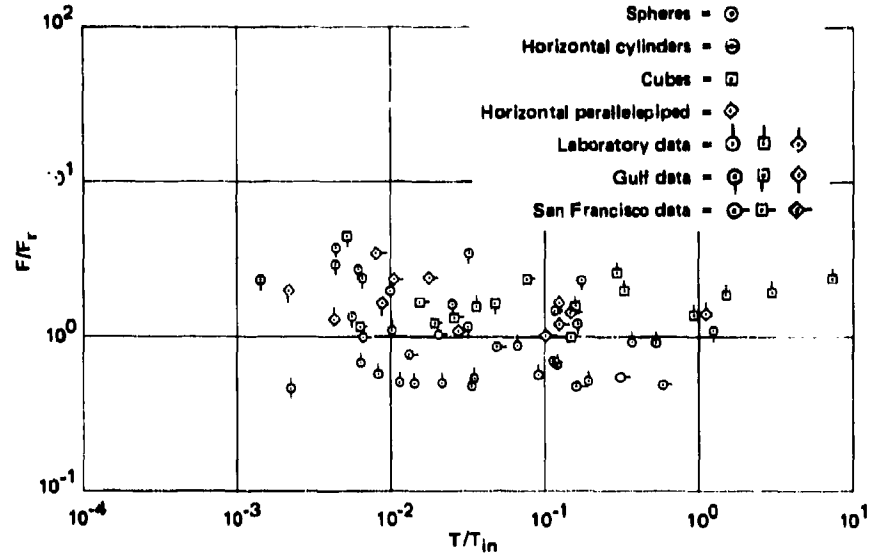

Figure 15. Breakout force correlation of experimental data.

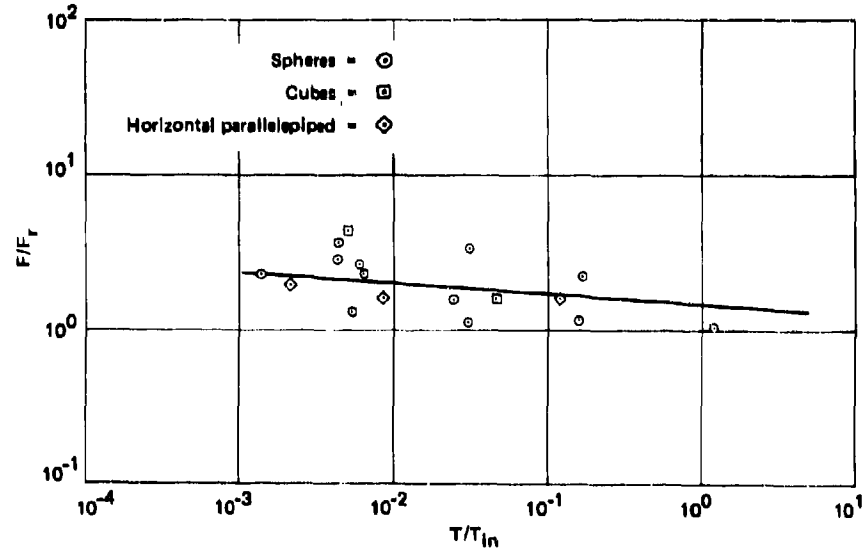

Figure 16. Breakout force correlation of Gulf of Mexico data only.

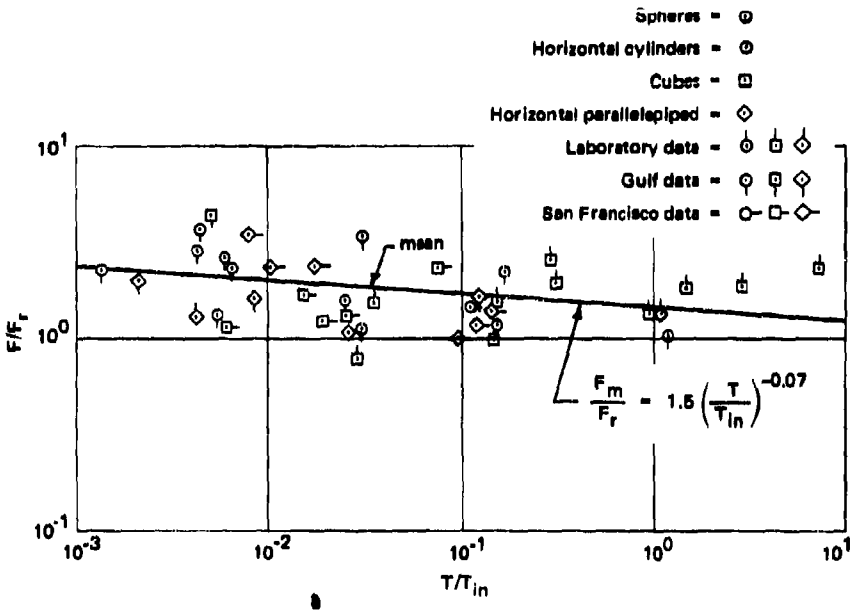

Figure 17. Breakout force correlation of corrected data points.

The derivation of Liu's correlation is based upon a sound understanding of the breakout mechanism and the dimensional analysis. Even though the correlation fails to take into account the breakout force recession characteristics of the object and the soil creeping characteristics, all data have the F/F_r values at the same order of magnitude, as shown in Figure 17.

Correlation Characteristics

Like any other soil problem, the breakout phenomenon contains a large number of uncertainties. But there is a definite general trend which can be identified from the experimental results. The breakout time is very sensitive with respect to the breakout force. A small change in the value of F/F_r will result in a great difference in T/T_{in}. With the large number of uncertainties involved, it is almost impossible to predict with any degree of accuracy when an object will be pulled out. Fortunately, in most of the engineering problems related to this subject it is not necessary to pinpoint the breakout time; usually the maximum breakout time is specified, for example, as in a rescue mission. To assure an early breakout, a factor of safety can be applied to the breakout force. This force increase is not likely to create any heavy burden to the equipment, because a small increase in breakout force will reduce the breakout time appreciably.

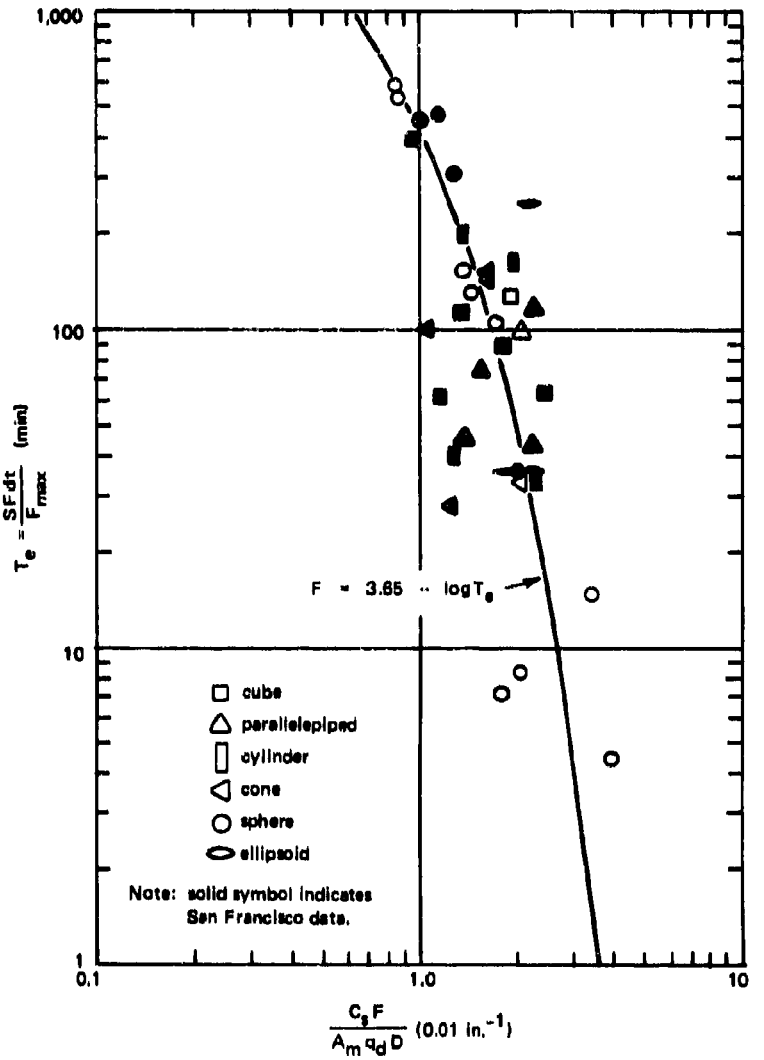

Figure 18. Breakout force results for field test data only.

The breakout force and breakout time seem to be related in the form of a power law:

$$\frac{F}{F_r} = C_1 \left(\frac{T}{T_{in}} \right)^{-C_2}$$

where C_1, C_2 = empirical constants having positive values. Thus, the equation is not valid for instant breakout, because at $T = 0$ the value of F becomes infinitely large, which seems to be impossible. However, for an instant breakout in a real situation, the breakout time is not equal to zero but to a finite short time period, such as the time required for the applied force to reach its peak value. The value of F/F_r for such rapid breakout is in general less than 10, as shown in Figure 17. An instant breakout will result if the net breakout force is at least 10 times the soil resistance.

The experimental data has a wide scattering range. Many mathematical equations would fit the data to about the same degree of accuracy. But for simplicity a power law form is chosen to fit the data by eye. The mean value of the corrected data points may be represented by the equation

$$\frac{F_m}{F_r} = 1.5\left(\frac{T}{T_{in}}\right)^{-0.07} \qquad \text{for } 10^{-3} < T/T_{in} < 10 \qquad (6)$$

The scattering of the data points is best described by a probability characteristics curve, as shown in Figure 19. The maximum value of F/F_r is 2.1 times that of the mean value, F_m/F_r. The probability of successful breakout for this F/F_r value is 100%. The minimum value of F/F_r that causes a breakout is 0.42 times that of the mean and breakout will probably not occur. Therefore, any value of F/F_r may be evaluated based on the factor of safety, which is the ratio of the breakout force to the calculated mean.

The following observations may be drawn from the breakout force correlations:

1. F/F_r depends very weakly on T/T_{in}.
2. Larger breakout forces are required for square-edged objects.
3. F/F_r scattering is about 160%. It is not possible to determine exactly a relationship between F/F_r and T/T_{in} at this stage.
4. The correlation in Figure 17 may be roughly represented by $F_m/F_r = 1.5\,(T/T_{in})^{-0.07}$.
5. The necessary condition for breakout to occur is at least $F/F_m = 2.1$. The necessary condition for breakout not to occur is $F/F_m = 0.42$ or less.
6. It is not practical to predict the time for breakout.

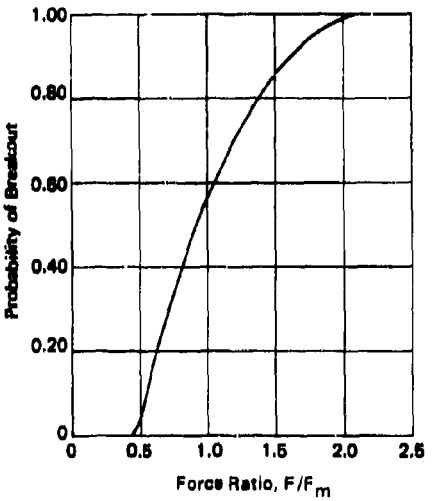

Figure 19. Probability characteristics of the experimental data.

Breakout Observation

The model study soil before breakout is shown in Figure 20. As the 2.5-inch sphere was sinking into the test soil, soft mud was observed being squeezed along the solid wall out to the surface. A ring with radial hairline cracks formed in the soil. The soil also bulged slightly about the sunken sphere, but gradually flattened. It appeared that the soil at the surface was too soft to resist shear strain. After the sphere was pulled out, the soil pattern suggested an adhesion failure rather than a cohesion failure. This is illustrated in Figure 21. Note that almost one-half of the failing surface is smooth; the other half would also be smooth if the rim of the crater did not tumble in. Evidently the lifting force was not exactly vertical. As the sphere was being pulled out the soil moved toward the center of the crater to fill the space left by the sphere. The circular cracks around the hole were caused by such movement.

A cube sinks into mud in the same way as a sphere, except that the excessive soil is squeezed out to form a ring of a different geometry. As can be seen in Figure 22 no hairline crack is visible. The 3-inch cube sank by its own weight. A sequence of pictures taken during the breakout is presented in Figures 22 through 25. The initial displacement was made without disturbing the surrounding soil. But as the displacement reached 1 inch, as shown in Figure 24, excessive soil movement caused a ring of cracks about the object, which indicates that the soil under the cube was also moving upward. There was apparently no soil attached to the cube wall. The bond between the soil and the top of the cube wall failed first, and the cube slid out from the soil. Figure 25 reveals the soil pattern right after breakout. The 3-inch cube has been replaced by at least 2.5 inches of soil, which probably did not cave in from the surface but flowed up by the pressure difference between the soil surface and the bottom of the cube. The crater is not smooth. The failure at the base of the cube must be a tension or cohesion failure.

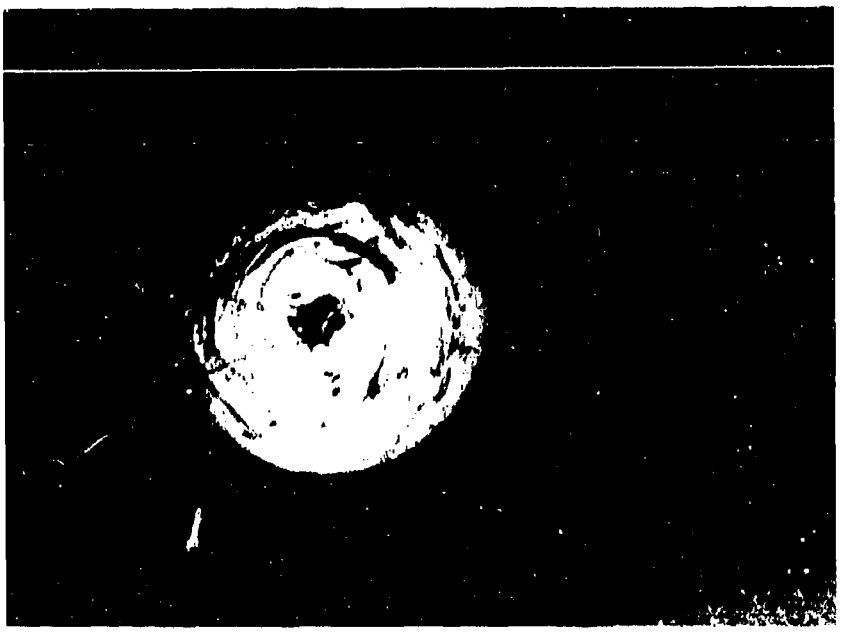

Figure 20. A 2.5-inch sphere after emplacement in test tank.

Figure 21. Crater left by 2.5-inch sphere after breakout.

Figure 22. A 3.0-inch cube after emplacement in test tank.

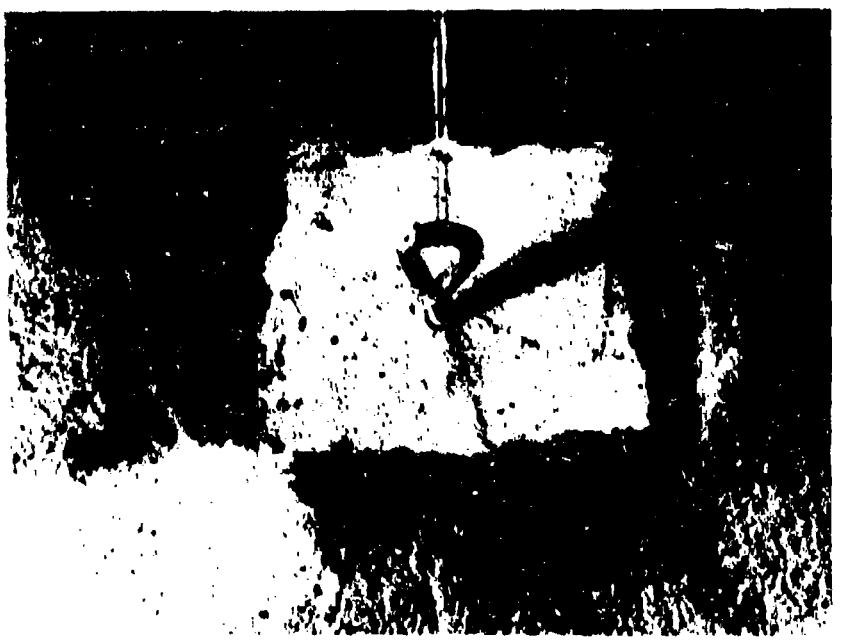

Figure 23. Cube is being pulled out to about 1/2 inch above surface.

Figure 24. Cube is being pulled out to about 1 inch above surface.

Figure 25. Soil surface after the cube has been pulled out.

Settlement Versus Cohesion

Tests were conducted to check the homogeneity of the test soil. Two objects were sunk into mud twice. The embedded depths were approximately similar for each emplacement. This resolves the doubt that embedment can be different for the same object placed into the same soil at different times. It also indicates that soil cohesion does not increase appreciably over a period of time, for instance 24 hours, which is the time interval between the emplacement of the objects.

Small-Scale Model Tests

The quality of the model test data was tested by comparison with the field test data. The data points seem to blend nicely with the field test data, but with slightly higher values. The scatter of the data points is smaller than that for the field tests. The model test data also cover a much larger range of T/T_{in} values. In general, the quality of the laboratory test data is considered better than that of the field test data.

Small-scale model tests can be performed at any time and can be reproduced as desired. The soil condition and the object geometry can be well controlled. The expense involved in the model test is small.

The disadvantage of the model test includes the difficulty in simulating the cohesion profile for the soil. It is also difficult to evaluate the effect of the size of the test object. But most of all, the data will be affected by the ever-changing strength of the remolded soil.

Rapid Pullout Tests

Data for the rapid pullout tests are presented in Table 3 and Figure 26. The breakout force appears to be about 10 times larger than the slow breakout data. Since the objects in these tests were plates with no side walls, the soil resistance calculations were based on tension strength under the plate alone. Actually the soil filled back on top of the plate after it was sunken. This is illustrated by a photograph taken during the small-scale laboratory tests (Figure 27). The object under the soil is a cube. Notice the soil has fallen back to the cavity created by the object. This filling back of soil will increase the damping of the net breakout force. The inertia of the mass and of the virtual mass becomes an additional resistance to the lifting of the test objects at high speeds. Then too, the net breakout force was calculated by using the peak of the rapidly applied load, which is expected to be higher than a constantly applied load having the same result. Maybe the largest contribution to the resistance comes from the suction at the bottom of the

plate, which is caused by too slow a seepage flow in the soil compared to the speed of pullout. Therefore, the high values of the breakout force are considered a result of the application of rapid force.

Table 3. Data Obtained From Rapid Pullout Tests

(Average soil cohesion = 0.09 psi.)

Plate Area, A_x ($in.^2$)	Net Breakout Force, F (lb)	Soil Resistance, F_r (lb)	Force Ratio, F/F_r	In-Situ Time, T_{in} (sec)	Breakout Time, T (sec)	Time Ratio, T/T_{in}
144	288	13.0	22.4	240	12.40	0.0515
255	464	22.9	20.2	201	5.67	0.0282
225	432	20.2	21.3	179	27.20	0.152
36	108	3.2	33.4	140	12.05	0.086
63.7	144	5.7	25.0	153	8.15	0.053
177	336	15.9	21.1	89	20.15	0.225
177	324	15.9	20.3	93	18.60	0.200
28.2	48	2.5	18.9	121	19.68	0.163
113	264	10.2	26.0	91	6.24	0.0685

ERROR ANALYSIS

Instrument

The dynamometer was carefully calibrated before the tests and was checked occasionally thereafter. It had an error of 5%. The force record can be read to an accuracy of 500 pounds, which may cause as much as a 30% error for F/F_r. The displacement indicator was damaged several times. The embedment measurement, which was made by the divers, is estimated to be in error by 10%. This may cause the ratio F/F_r to be off by 10%. The maximum instrument error, then, should be less than 40%.

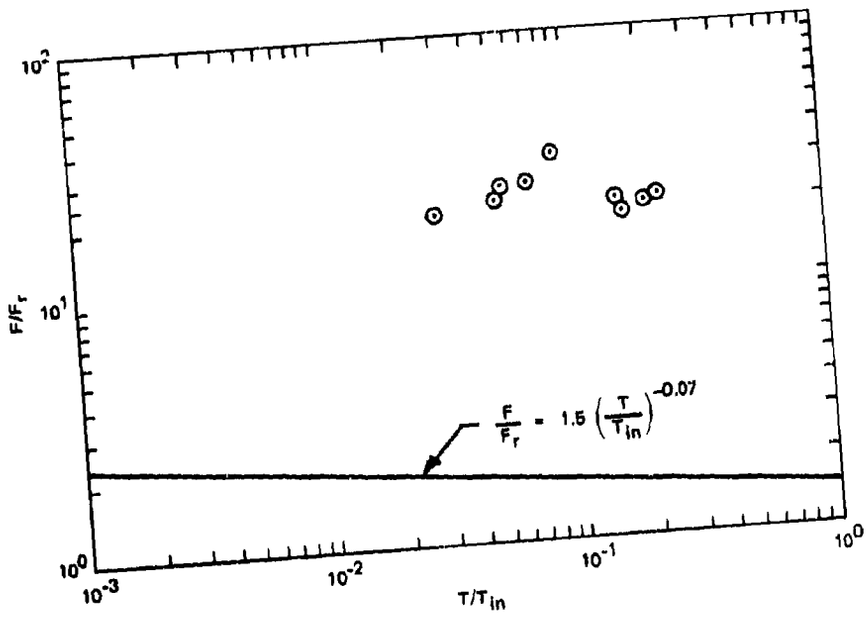

Figure 26. Rapid pullout test results.

Figure 27. Object covered by the backfilling soil.

Lifting Force

The force applied to the object, even though it is provided by a pair of pontoons, cannot be kept constant. The subsurface current has two effects on the uplifting force. First, the pontoons are forced to swing and oscillate. This action periodically increases the lifting force. Second, the pontoons tend to drift downstream of the average current. The force then acts on the object at an angle and thus complicates the bonding condition around the object.

In 100 feet of water the position of the object in soil cannot be controlled. In most cases the object will land and sink at a slight inclination. This is especially true for the sphere. The application point of pull (where the pulling line is attached) may not be positioned just above the center of gravity of the object. When the object is pulled out, a moment is created which helps to break the object–soil bond and greatly reduces the soil resistance. This force eccentricity will, in general, reduce the breakout time. But for a deeply embedded object having sharp-angled edges, the eccentricity of the force may cause an increase in side friction.

Soil Cohesion

It is not feasible to take in-situ vane shear readings at every test site before the test. The core samples of the test area were taken before the test actually started. The cores were brought to shore for vane shear tests about half a day after they were taken from the site. The resulting vane shear strength profile is somewhat irregular on some samples. The error of the profiles themselves is about 10-20% due to the difficulty of reading the instrument. Only six soil profiles are available from the test area. Interpolation and extrapolation are necessary to estimate the cohesion at the test sites. These values of cohesion were used in data reduction. An additional 10% error may be involved. The uncertainty about the soil surface condition, such as depression, shell layers, and hardpan, implies another possibility of error in estimating cohesion. The vertical distribution of the cohesion often is not linear as assumed in the calculation. Yet another 10% error may be involved in estimating average cohesion ($\bar{c}$)

Soil Stress Creeping, Viscosity, Permeability

The present correlation has completely neglected the effect of dynamic damping once the pullout motion has begun. There is no measurable quantity to represent the effect of stress creeping in saturated soil. The viscosity of the soil has not been properly defined. The effect of ground water flow was not investigated. All these uncertainties could be responsible for the large scattering of the test data.

Data Reduction

It is very difficult and time consuming to calculate the soil resistance for spherical and circular cylindrical objects partially embedded in soft bottom soils without making bold assumptions. The failure prism assumption is responsible for errors occurring on nonprism objects.

The definition of effective time (T_e) is based on a linear force--time relationship. But the resultant correlation indicates a near-logarithmic function.

APPLICATION OF TEST RESULTS

The empirical correlation curve in Figure 17 may be used directly for the estimate of the breakout forces required to lift from the sea floor such objects as a cube, a sphere, a horizontal cylinder, a parallelepiped, and the like, having relatively smooth surfaces. The engineer should first collect the following data:

1. Submerged weight and external configuration of the sunken object.
2. Soil vane shear strength profiles at the site.
3. Time of embedment.

Estimate the submerged weight of the sunken object as accurately as possible. The buoyancy force produced by the soil should be included. Take into account the possible water and soil leakage through any possible punctures in the object hull. The soil resistance is evaluated in three steps. First, determine a failure prism. This surface will coincide with the object surface if the embedded configuration is of a prism form. In nonprism cases, the failure prism is one having a base area equal to the maximum object cross section in soil and a height equal to one-half of the embedment. For odd geometries, appropriate modifications should be made to the failure prism. The second step is to measure or estimate the vane shear strength at the depth of embedment. It is most desirable to measure the vane shear strength of the soil. However, if such an operation is not feasible, the value of the soil strength must be estimated as accurately as possible based on available references. The average vane shear strength profile shown in Figure 11 may be used as a guide for a quick estimate. With the cohesion value determined, the next step is to calculate the soil resistance force by Equation 5. Then either breakout time or breakout force may be specified and the other one determined with the help of Figure 17.

The following examples illustrate the use of the test results.

Example 1. A 3,000-pound dry weight concrete parallelepiped having a 2 x 2-foot cross section and a 5-foot length was sunk horizontally a week ago into the ocean floor about 1 foot deep under 100 feet of water. What is the minimum force required to pull the parallelepiped out of the soil within 1 hour? No information is obtainable on local soil strength, but the mud attached to the anchor appears to be very sticky fine clay.

List the above information in order:

1. Dry weight: 3,000 pounds

   Soil weight density: unknown

   Object configuration under soil: 2 x 5 x 1-foot prism

2. Soil vane shear profile at site: unknown

   Soil type: fine clay

3. Time of embedment: 1 week

The submerged weight is first calculated after assuming that the net weight of the clay is 100 lb/ft^3; the average cohesion of the soil between the soil surface and the depth of embedment is about 37 psf based on Figure 11. The soil resistance is

$$F_r = 37\,[2(5) + 2(2+5)(1)] = 888 \text{ pounds}$$

The in-situ time of the object is 10,080 minutes, and the specified breakout time is 60 minutes. Therefore,

$$\frac{T}{T_{in}} = \frac{60}{10{,}080} = 0.00595$$

From the mean curve in Figure 17 or from Equation 6, the corresponding value of F/F_r is seen to equal 2.1. From Figure 19 a 100% probability of breakout establishes a force factor of 2.1. Thus

$$F = (2.1)(2.1)(F_r) = (4.41)(888) = 3{,}920 \text{ pounds}$$

The buoyancy force is

$$B = 64.0(2 \times 5 \times 1) + 100(2 \times 5 \times 1) = 1{,}640 \text{ pounds}$$

The necessary gross lifting force is

$$F_a = 3{,}000 + 3{,}920 - 1{,}640 = 5{,}280 \text{ pounds}$$

This is the minimum uplifting force required for breakout within an hour.

Example 2. The submersible research vessel *Alvin* has been resting on the bottom soil in 5,000 feet of water for 1 hour. Both keels have been buried 6 inches in the mud. The vessel's negative buoyancy during this time period was 1,000 pounds. What is the uplifting force required to free it from the bottom mud within 10 minutes?

Since the bottom condition is not specified, let us assume that the cohesive strength of the bottom soil 6 inches from the surface is 39 psf, in accordance with Figure 11. The average cohesion may be taken as 20 psi.

The dimension of the two keels may be approximated by two parallelepipeds 6 inches wide and 10 feet long. Therefore, the soil resistance is

$$F_r = 20\left[2\left(\frac{1}{2}\right)(10) + 2(2)\left(10 + \frac{1}{2}\right)\right] = 1{,}040 \text{ pounds}$$

The resting time (T_{in}) is 60 minutes, and the specified breakout time (T) is 10 minutes. The ratio $T/T_{in} = 1/6 = 0.167$. From Equation 6 or Figure 17 it is found that $F/F_r = 1.70$ and $F = 1.70\ (F_r) = 1.70\ (1{,}040) = 1{,}770$ pounds. The object buoyancy is

$$B = (100 - 64)\left(\frac{1}{2}\right)(10)\left(\frac{1}{2}\right)(2) = 180 \text{ pounds}$$

$$F_a = 1{,}000 - 180 + 1{,}770 = 2{,}590 \text{ pounds}$$

A total of 2,590 pounds of uplift force is needed to free *Alvin* in 10 minutes. The probability of success is 56% when $F/F_m = 1.0$, according to Figure 19.

FINDINGS

1. A dimensionless correlation of the net breakout force with the breakout time has been selected for both field and model test data. The correlation is general enough for various soil conditions and object sizes. The correlation curve may be represented by an equation in the form of $Y = n_1 X^{n_2}$, where n_2 and n_1 are constants.

2. The necessary net breakout force required to break an object loose from the ocean floor within a specified time can be estimated from the empirical data. However, it is not possible to accurately predict the time of breakout, even though the net breakout force is given.

3. A small change in breakout force results in a great difference in breakout time.

4. The breakout force is a function of soil cohesion, object hull shape, cross-sectional area, time of embedment, time of breakout, and soil permeability. The hydrostatic pressure, object mass, surface roughness, soil density, and water properties are of little importance. The effects of soil viscosity, stress creeping in soil, seepage flow in soil, eccentricity, and rate of applied force require further investigation.

5. Small-scale laboratory tests have the following advantages:

   a. More affecting parameters, such as hydrostatic pressure, may be controlled.

   b. The experiment may be observed at any time under conditions of good visibility.

   c. The cost of equipment, material, and labor is only a fraction of that for a field test.

   d. The rate of data production is much faster than it is for a field test.

   e. The test time would not be affected by the weather.

   f. Data can be checked and reduced and the test repeated while the test conditions remain unchanged.

CONCLUSIONS

1. The experimental data are presented as a correlation between the dimensionless net breakout force (F/F_r) and the dimensionless breakout time (T/T_{in}). This correlation is best described by the equation

$$\frac{F_m}{F_r} = 1.5\left(\frac{T}{T_{in}}\right)^{-0.07} \qquad \text{for } 10^{-3} < T/T_{in} < 10 \qquad (6)$$

The range of the data scattering is about 150% of the mean values. The net breakout force may be estimated either by using the curve in Figure 17 or by using Equation 6. A safety factor of 2.1 should be applied in cases where a breakout must be achieved.

2. The breakout time, which is very sensitive to the breakout force, is extremely difficult to predict with any reasonable accuracy. The maximum error for predicting the net breakout force is determined on the basis of probability. Engineering judgment must be exercised when estimating breakout force.

3. Water jetting under embedded objects and lifting embedded objects from one end effectively reduces the resistance to uplift. The method of flooding under the hull completely eliminates the net breakout force.[1]

4. The error in the estimate of the net breakout force may be large due to the stratified soil or the different loading history during the field operation.

RECOMMENDATIONS

1. The empirical correlation in Figure 17 should not be considered as a final solution to the breakout problem, but rather as a logical guide for estimating breakout force for engineering purposes.

2. The small-scale model study should be adopted as a primary tool for collecting more breakout force data in the future.

3. The correlation should be improved by taking into account the effect of the changing soil buoyancy, the changing soil resistance during breakout, and the permeability of the soil.

4. Research should continue on finding a mathematical model for the breakout problem.

Appendix A

PROPERTIES OF SEDIMENT AT GULF TEST SITE AND IN LABORATORY TEST TANKS

by

Melvin C. Hironaka

The site for the breakout tests was selected on the basis of available information and personal communication with various cognizant agencies of the area, with various oil companies, and with consulting firms. As a result of these efforts, block 212 of the Eugene Island area in the vicinity of 28° 37.8'N and 91°21.2'W was selected to be surveyed (Figure A-1). The initial core samples indicated that the sediments were exactly the cohesive type desired for the tests. The water depth was also satisfactory. Thus, the survey of block 212 was carried through to completion.

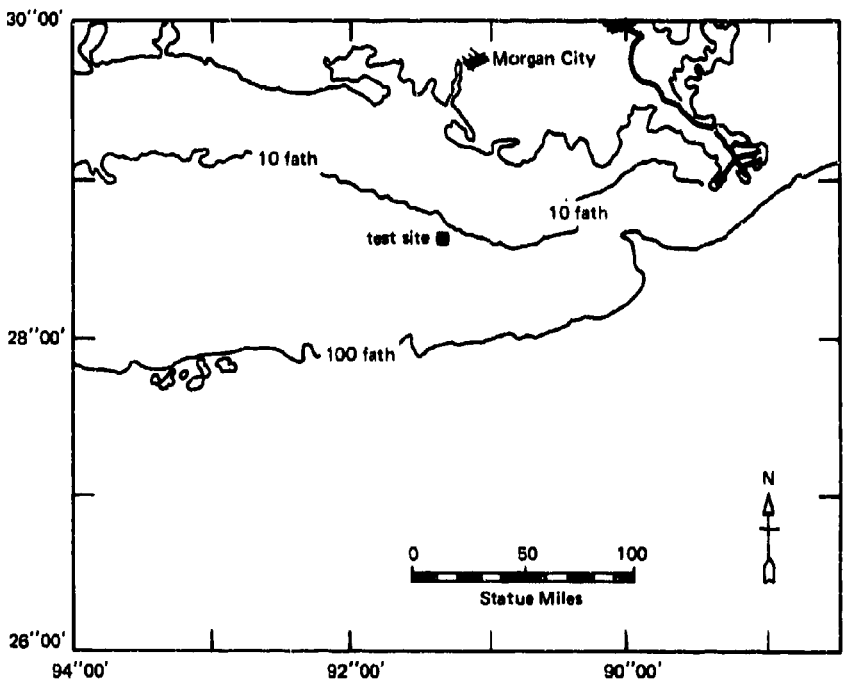

Figure A-1. Location of the test site in the Gulf of Mexico.

The USNS *Sands* (T-AGOR 6) was used in conducting the survey. The detailed bathymetric survey was performed with a UQN fathometer and with radar bearings and distances from various established platforms in the vicinity of block 212. With the collected data, the bathymetric chart of the test site was prepared (Figure A-2).

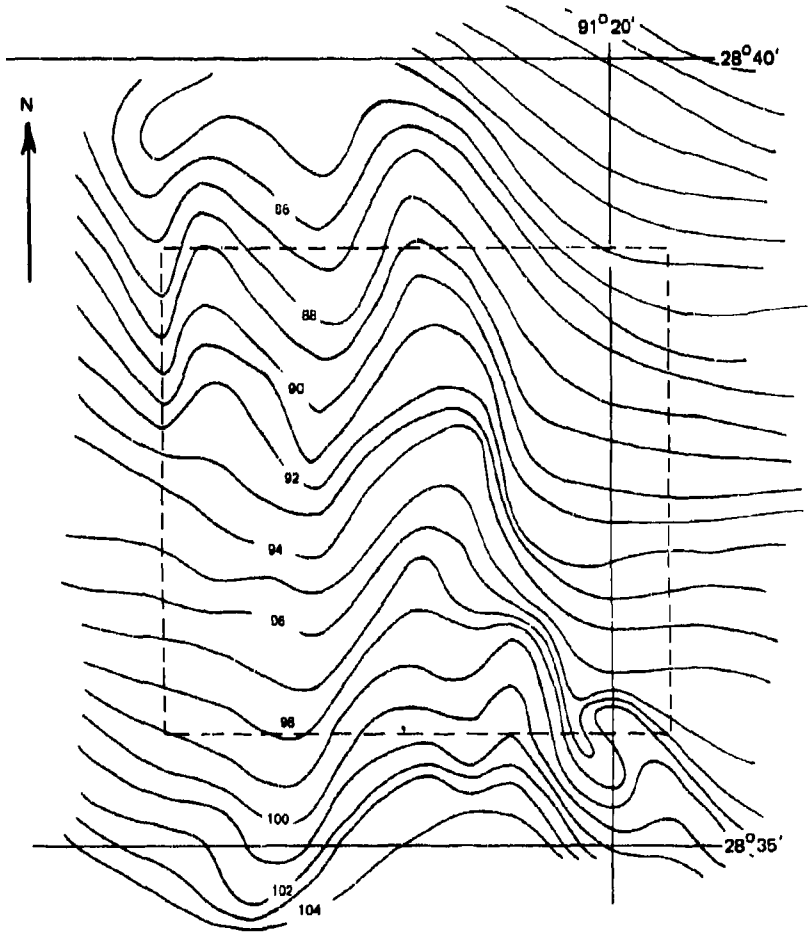

Figure A-2. Bathymetric chart of the test site.

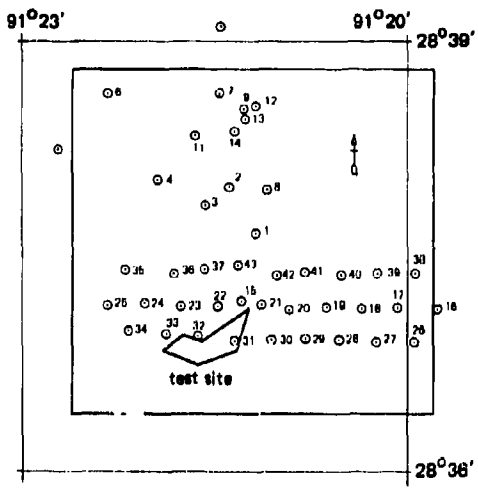

Figure A-3. Location of core samples relative to the boundaries of block 212.

Using the same positioning techniques, the vessel was maneuvered into preselected positions and the core sampling was initiated. A total of 43 attempts was made to obtain core samples at the site; a 400-pound Ewing-type corer equipped with a piston and a cellulose acetate butyrate liner was used. The initial core samples were extruded on the deck to certify that the sediments were uniform with depth and of the desired type. Figure A-3 shows the location of the core samples with respect to the boundaries of block 212.

Although the vessel was equipped with a bow thruster, the wind, currents, and seas approaching the vessel simultaneously from different directions made it very difficult to keep the vessel on station. The drift of the vessel, coupled with the vertical oscillations due to the seas, made it very difficult to extract the corer from the sediment at a slow enough rate to prevent crushing the plastic liner and disturbing the sample. Thus, many of the samples were severely disturbed towards the top.

Simultaneously with the sampling operations, selected segments of each core were tested for vane shear strength aboard the vessel with the laboratory vane shear described in Reference 6. Some problems were encountered which influenced the performance of these tests aboard the vessel. The occasional vibrations caused by the starting of the main engines and the pitch and roll due to the seas caused some of the samples undergoing tests to fail prematurely. The remaining segments of each core were capped and sealed for additional tests and evaluation ashore.

A portion of the remaining segments of the samples was tested for bulk wet density and original water content at the New Orleans district facility of the Corps of Engineers. The remaining tests and core logging were completed at NCEL.

The results of these tests for the samples taken in the vicinity of the specific locale in which the breakout tests were conducted are summarized in Tables A-1 to A-7. Since there are different basic definitions for some of the derived values shown and space is limited here, the reader is referred to

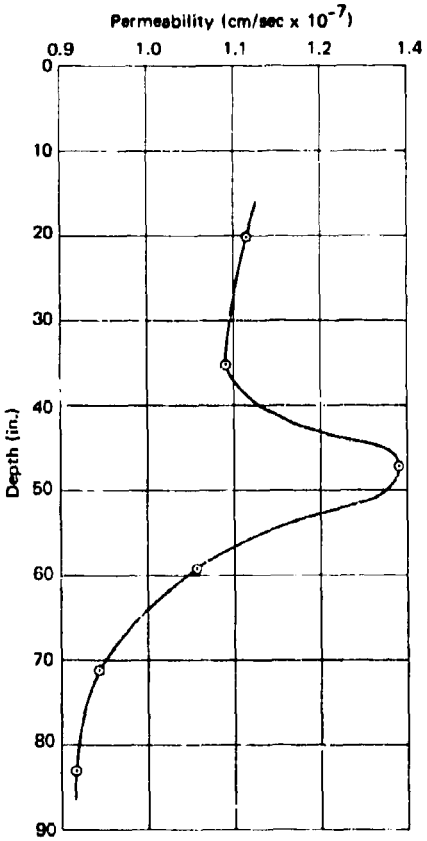

Figure A-4. Coefficient of permeability versus depth for core taken from Gulf of Mexico.

to Reference 7 for the definitions used to obtain the various values. In addition, the results of permeability tests conducted on sample 32 are summarized in Figure A-4. This is the only sample that was subjected to permeability tests. The values of permeability were corrected for the temperature of the water at the bottom, 19.4°C, which is the approximate average value observed by the divers during breakout tests. The effect of the small pockets and thin layers of sand and silt on permeability is negligible since they are, in a sense, floating in the silty clay matrix and their size is small relative to the sediment mass.

An important observation of the bottom by the divers during the breakout tests should be noted. The undisturbed sediment surface was not smooth and uniform, but was fractured in a hexagonal-shaped pattern similar to the patterns resulting from a desiccating mud lake. The fractures in places were as large as 2 inches wide and 8 inches deep. The presence of these fractures indicates that the breakout phenomena in this area will not be satisfactorily represented by considering the sediment as a continuous and viscoelastic material. The scattered depressed areas had a very soft covering, which was as thick as 12 inches in places.

In summary, the site surveyed is nearly flat with an average slope of approximately 6 ft/mile. The samples retrieved were generally uniform silty clay, with the exception of some samples which contained small pockets and thin layers of fine sand and silt. Vane shear strengths increased with depth in the sediment. Minimum strengths which occurred at the sediment surface were not measurable with the device indicated. Maximum strengths were in the range of 300 to 350 psi. The sediments appear to become firmer and

more consolidated towards the northern boundary of the area. The coefficient of permeability is small for the silty clay matrix of the sediment, the average coefficient being about 1.2×10^{-7} cm/sec.

The soils were sampled in two of the test tanks for model studies. Several cores were taken at various times. The soil properties are presented in Tables A-8 and A-9. The grain size distribution curves are shown in Figures A-5 and A-6. Most of the breakout test data were obtained in Seal Beach soil. Because the Point Mugu soil contained too much organic debris, it represented a poor simulation of a deep ocean bottom sediment.

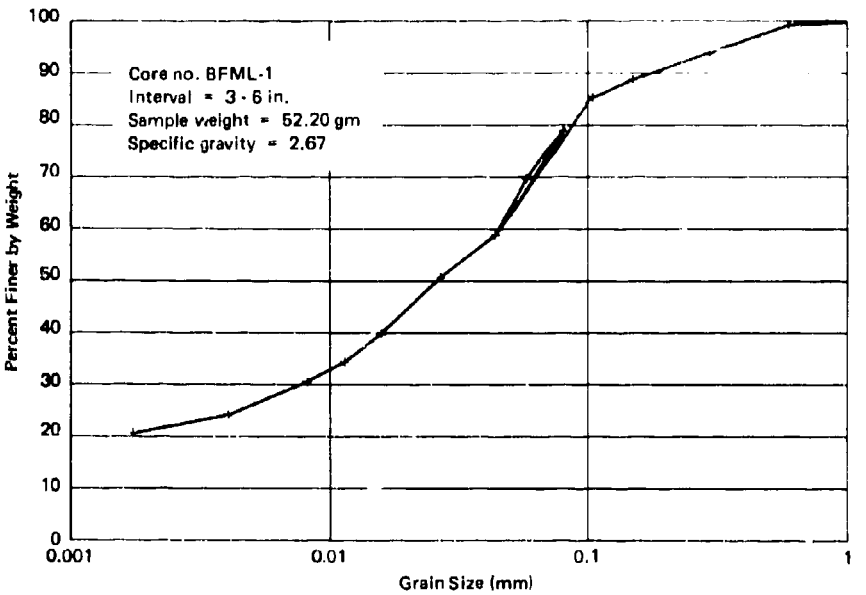

Figure A-5. Grain size distribution for Seal Beach soil.

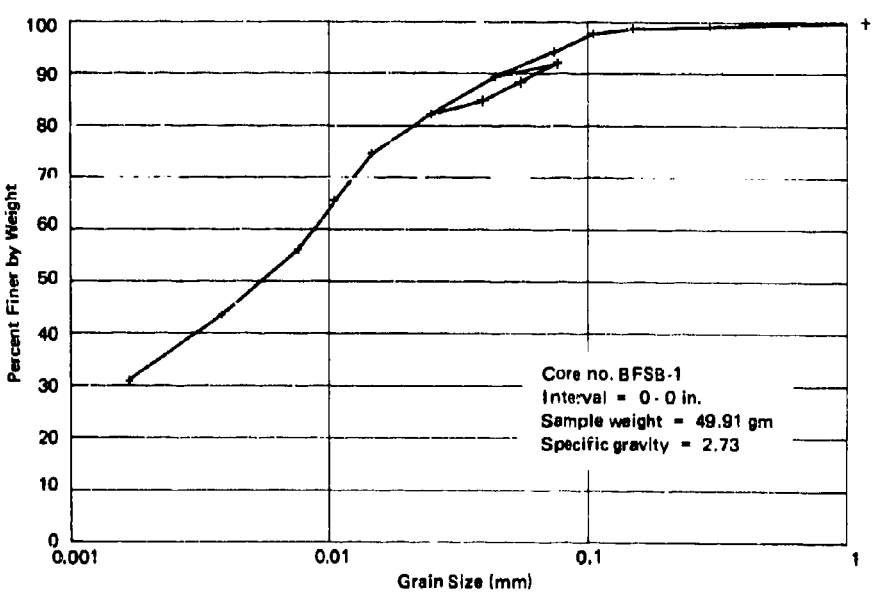

Figure A-6. Grain size distribution for Mugu soil.

LATITUDE [illegible] N	LONGITUDE 91 21.15 W			WATER DEPTH		96. FT	
INTERVAL (IN)	0- 3	12-15	24-27	36-39	48-51	60-63	72-75	84-87
COLOR (5YR NO.)	[illegible]	[illegible]	[illegible]	[illegible]	5Y4/1	5GY4/1	5GY4/1	5GY4/1
ODOR	H2S	H2S	H2S	H2S	H2S	H2S	H2S	H2S
BULK WET DENSITY (PCF)		105.		101.		102.		104.
VANE SHEAR STRENGTH (PSF)	11.		187.		100.		267.	-
REMOLDED STRENGTH (PSF)	11.		60.		67.		141.	-
SENSITIVITY	1.0		2.7		1.6		1.9	-
ORIGINAL WATER CONTENT (P)*		61.0		67.1		69.6		61.3
SPECIFIC GRAVITY OF SOLIDS		2.67		2.69		2.69		2.71
DRY DENSITY (PCF)		65.		60.		60.		65.
VOID RATIO		1.55		1.78		1.79		1.60
POROSITY (P)		60.7		64.0		64.2		61.5
SATURATED VOID RATIO		1.63		1.81		1.87		1.66
LIQUID LIMIT (P)		58.		68.		74.		69.
PLASTIC LIMIT (P)		25.		33.		30.		36.
PLASTICITY INDEX		33.		35.		44.		33.
LIQUIDITY INDEX		108.		98.		89.		76.
COMPRESSION INDEX		.49		.52		.58		.53
CARBONATE CARBON CONTENT (P)		.41		.33		.27		.44
ORGANIC CARBON CONTENT (P)		.48		.53		.52		.50
SAND (P)		15.0		2.8		3.3		.4
SILT (P)		35.0		34.9		29.8		27.4
CLAY (P)		50.0		62.3		66.9		72.2
ACTIVITY		.8		.7		.8		.6
MEDIAN DIAMETER (MM)		.0050		.0014		.0015		.0000
SEDIMENT TYPE		SILTY CLAY		SILTY CLAY		SILTY CLAY		SILTY CLAY
MICROSCOPIC ANALYSIS - PLUS 325 MESH FRACTION.(P)								
QUARTZ		80		75		80		80
BENTHONIC FORAMINIFERA		5		10		5		10
ASPHALT		5		2		2		5
BIOTITE		1		1		1		2
MUSCOVITE		1		2		1		1
SHELL FRAGMENTS		5		1		8		2
PLANKTONIC FORAMINIFERA		1		1		-		
OTHER MINERALS		2		1		2		
WAX FRAGMENTS		-		5		-		
ORGANIC MATERIAL		-		2		1		

REMARKS***
THE GENERAL COLOR IS DARK GREENISH GRAY EXCEPT FOR THE INTERVAL 27-51 INCHES WHICH IS OLIVE GRAY. SOME BLACK MOTTLING PRESENT BETWEEN LINER AND SAMPLE. SMALL POCKETS OF FINE SAND SCATTERED THROUGHOUT THE SILTY CLAY MATRIX. A LAYER 4 INCHES THICK OF FINE SAND BEGINS AT 56 INCHES. A POCKET OF SHELL FRAGMENTS OCCUR AT 64 INCHES. BETWEEN 36 AND 53 INCHES, THE SAMPLE APPEARS TO BE DISTURBED. AT 51.5 INCHES A HORIZONTAL SEPARATION APPROXIMATELY 3/8 INCH THICK IS OBSERVED.

Table A-2. Summary of Test Results for Core 21 in Gulf of Mexico.

LATITUDE 18 37.50 N	LONGITUDE 91 21.15 W			WATER DEPTH		96. FT		
INTERVAL (IN)	0- 3	12-15	24-27	36-39	48-51	60-63	72-75	84-87	90-93
COLOR (5YR NO.)	5GY4/1	5GY4/1	5GY4/1	5GY4/1	5Y4/1	5Y4/1	5GY4/1	5GY4/1	5GY4/1
ODOR	H2S	H2S	H2S	H2S	H2S	H2S	H2S	H2S	H2S
BULK WET DENSITY (PCF)		102.		104.		99.		105.	
VANE SHEAR STRENGTH (PSF)	11.		117.		240.		262.		164.
REMOLDED STRENGTH (PSF)	9999.		59.		71.		119.		123.
SENSITIVITY	9999.9		2.0		3.7		2.2		1.3
ORIGINAL WATER CONTENT (P)*		67.4		64.7		74.8		62.0	
SPECIFIC GRAVITY OF SOLIDS		2.72		2.69		2.74		2.67	
DRY DENSITY (PCF)		61.		63.		57.		65.	
VOID RATIO		1.77		1.67		2.02		1.57	
POROSITY (P)		63.9		62.6		66.9		61.2	
SATURATED VOID RATIO		1.89		1.74		2.05		1.66	
LIQUID LIMIT (P)		69.		72.		80.		67.	
PLASTIC LIMIT (P)		35.		36.		40.		35.	
PLASTICITY INDEX		34.		36.		40.		32.	
LIQUIDITY INDEX		95.		80.		87.		85.	
COMPRESSION INDEX		.53		.56		.65		.51	
CARBONATE CARBON CONTENT (P)		.41		.29		.21		.22	
ORGANIC CARBON CONTENT (P)		.52		.62		.56		.56	
SAND (P)		14.0		1.3		.8		4.7	
SILT (P)		35.2		37.1		24.1		33.2	
CLAY (P)		50.8		61.6		75.1		62.1	
ACTIVITY		.8		.7		.7		.6	
MEDIAN DIAMETER (MM)		.0047		.0019		.0010		.0018	
SEDIMENT TYPE		SILTY CLAY		SILTY CLAY		CLAY		SILTY CLAY	
MICROSCOPIC ANALYSIS - PLUS 325 MESH FRACTION.(P)									
QUARTZ		80		50		50		60	
BENTHONIC FORAMINIFERA		10		20		15		20	
OTHER MINERALS		5		5		5		10	
ASPHALT		2		2		1		5	
ORGANIC MATERIAL		1		10		5		4	
SPICULES		1		1		1		1	
MICA		1		10		10			
PLANKTONIC FORAMINIFERA		-		2		3			
AGGREGATES		-		-		10			

REMARKS***
THE SAMPLE IS DARK GREENISH GRAY EXCEPT FOR THE INTERVAL 48-64 INCHES WHICH IS OLIVE GRAY. SOME BLACK MOTTLING BETWEEN LINER AND SAMPLE. FROM 39 TO 46 INCHES IS A 3/4 INCH WIDE MOTTLED VERTICAL STREAK. SCATTERED SMALL POCKETS OF FINE SAND PRESENT IN THE SILTY CLAY MATRIX BETWEEN THE INTERVAL 51 TO 82 INCHES. FEW SHELL FRAGMENTS IN THE TOP 42 INCHES. NO VISIBLE LAYERING. THE BOTTOM OF THE SAMPLE APPEARS DISTURBED.

[illegible]

Table A-4. Summary of Test Results for Core 30 in Gulf of Mexico.

LATITUDE 28 37.22 N	LONGITUDE 91 21.09 W			WATER DEPTH			95. FT
INTERVAL (IN)	12-15	24-27	36-39	48-51	60-63	72-75	84-87
COLOR (GSA NO.)	5GY4/1	5GY4/1	5GY4/1	5GY4/1	5GY4/1	5GY4/1	5GY4/1
ODOR	H2S	H2S	H2S	H2S	H2S	H2S	H2S
BULK WET DENSITY (PCF)	99999.		101.		106.		101.
VANE SHEAR STRENGTH (PSF)		81.		185.		246.	
REMOLDED STRENGTH (PSF)		27.		65.		57.	
SENSITIVITY		3.0		2.5		4.3	
ORIGINAL WATER CONTENT (P)*	61.6		65.5		60.9		64.2
SPECIFIC GRAVITY OF SOLIDS	2.70		2.70		2.70		2.69
DRY DENSITY (PCF)	99999.		61.		66.		60.
VOID RATIO	999.99		1.75		1.56		1.82
POROSITY (P)	9999.9		63.7		61.0		64.5
SATURATED VOID RATIO	1.66		1.77		1.64		1.86
LIQUID LIMIT (P)	65.		65.		69.		73.
PLASTIC LIMIT (P)	29.		29.		30.		33.
PLASTICITY INDEX	36.		36.		39.		40.
LIQUIDITY INDEX	91.		100.		79.		90.
COMPRESSION INDEX	.49		.50		.53		.57
CARBONATE CARBON CONTENT (P)	.40		.27		.30		.32
ORGANIC CARBON CONTENT (P)	.48		.61		.46		.52
SAND (P)	17.3		2.0		7.0		2.6
SILT (P)	31.3		42.0		38.4		30.1
CLAY (P)	51.4		56.0		59.6		67.3
ACTIVITY	.8		.8		.8		.7
MEDIAN DIAMETER (MM)	.0044		.0030		.0021		.0013
SEDIMENT TYPE	SILTY CLAY		SILTY CLAY		SILTY CLAY		SILTY CLAY
MICROSCOPIC ANALYSIS - PLUS 325 MESH FRACTION.(P)							
QUARTZ	80		75		75		70
OTHER MINERALS	10		5		5		-
FORAMINIFERA	5		5		4		10
MICA	3		10		10		5
SPICULES	1		3		TR		TR
ASPHALT	1		1		TR		TR
SPONGE	TR		TR		-		-
ORGANIC MATERIAL	TR		1		5		15
SHELL FRAGMENTS	-		TR		1		TR

REMARKS***
THIS SAMPLE IS A FAIRLY UNIFORM DARK GREENISH GRAY SILTY CLAY. APPROXIMATELY 1.5 INCH THICK HORIZONTAL LAYERS OF FINE SAND ARE PRESENT AT 45.53, AND 81 INCHES. SMALL POCKETS OF FINE SAND ARE DISTRIBUTED BETWEEN 15-24 AND 39-45.5 INCHES. FEW SCATTERED SHELL FRAGMENTS IN TOP 36 INCHES. FROM 0-12 INCHES, THE SAMPLE IS HIGHLY DISTURBED DUE TO THE CRUSHING OF THE PLASTIC LINER DURING SAMPLING. SOME BLACK MOTTLING PRESENT BETWEEN LINER AND SAMPLE.

Table A-5. Summary of Test Results for Core 31 in Gulf of Mexico.

LATITUDE 28 37.24 N	LONGITUDE 91 21.66 W			WATER DEPTH 96 FT						
INTERVAL (IN)	0- 3	9-12	12-15	21-24	24-27	36-39	48-51	60-63	72-75	84-87	90-93
COLOR (GSA NO.)	5GY4/1	5GY4/1	5GY4/1	5GY4/1	5GY4/1	5GY4/1	5GY4/1	5GY4/1	5GY4/1	5GY4/1	5GY4/1
ODOR	H2S	H2S	H2S	H2S	H2S	H2S	H2S	H2S	H2S	H2S	H2S
BULK WET DENSITY (PCF)		99999.		101.		103.		105.		100.	
VANE SHEAR STRENGTH (PSF)	99999.		34.		133.		163.		147.		319.
REMOLDED STRENGTH (PSF)	9.		24.		100.		58.		77.		91.
SENSITIVITY	9999.9		1.5		1.3		3.2		1.9		6.0
ORIGINAL WATER CONTENT (P)*		66.2		69.8		49.4		60.5		68.0	
SPECIFIC GRAVITY OF SOLIDS		2.71		2.71		2.71		2.69		2.71	
DRY DENSITY (PCF)		99999.		59.		69.		65.		60.	
VOID RATIO		999.99		1.85		1.46		1.57		1.84	
POROSITY (P)		9999.9		65.0		59.4		61.2		64.7	
SATURATED VOID RATIO		1.79		1.89		1.34		1.62		1.84	
LIQUID LIMIT (P)		66.		71.		51.		67.		79.	
PLASTIC LIMIT (P)		27.		33.		29.		29.		33.	
PLASTICITY INDEX		37.		38.		21.		38.		60.	
LIQUIDITY INDEX		106.		98.		85.		92.		87.	
COMPRESSION INDEX		.48		.55		.19		.48		.57	
CARBONATE CARBON CONTENT (P)		.34		.35		.18		.27		.50	
ORGANIC CARBON CONTENT (P)		.48		.49		.32		.52		.93	
SAND (P)		12.1		1.4		6.7		2.0		.5	
SILT (P)		35.2		35.9		48.6		45.6		36.7	
CLAY (P)		52.7		62.7		44.7		52.4		64.8	
ACTIVITY		.8		.7		.6		.8		.7	
MEDIAN DIAMETER (MM)		.0040		.0019		.0084		.0080		.0015	
SEDIMENT TYPE		SILTY CLAY		SILTY CLAY		CLAYEY SILT		SILTY CLAY		SILTY CLAY	
MICROSCOPIC ANALYSIS - PLUS 325 MESH FRACTION.(P)											
QUARTZ		80		70		85		75		55	
OTHER MINERALS		5		10		3		15		10	
MICA		5		15		10		5		5	
ORGANIC MATERIAL		5		2		1		2		TR	
SHELL FRAGMENTS		2		-		-		3		20	
FORAMINIFERA		2		3		1		TR		10	
SPICULES		1		TR		TR		TR		TR	
ASPHALT		TR		TR		TR		TR		-	
REMARKS***								TR		TR	

THE COLOR OF THIS SAMPLE IS A UNIFORM DARK GREENISH GRAY WITH SOME BLACK MOTTLED AREAS BETWEEN THE LINER AND THE SAMPLE. SAMPLE IS GENERALLY A SILTY CLAY WITH 3/4 INCH DIAMETER POCKETS OF SAND AT 5 AND 82 INCHES AND VERY SMALL SCATTERED POCKETS OF SAND IN INTERVALS 15-21 AND 40-53 INCHES. FEW VERY SMALL SHELL FRAGMENTS IN 1-9 INCH INTERVAL. TOP 9 INCHES HIGHLY DISTURBED DUE TO CRUSHING OF THE LINER DURING SAMPLING. AT 35 INCHES, A CAVITY 3/8 INCH DIAMETER AND 1.5 INCHES LONG APPEARS TO HAVE BEEN CONSTRUCTED BY A BURROWING ANIMAL. AT 46 INCHES, A 1/8 INCH HORIZONTAL SEPARATION OF THE SAMPLE IS PRESENT.

Table A-6. Summary of Test Results for Core 32 in Gulf of Mexico.

LATITUDE 28 37.24 N	LONGITUDE 91 21.66 W			WATER DEPTH 96. FT						
INTERVAL (IN)	0- 3	9-12	12-15	21-24	24-27	36-39	48-51	60-63	72-75	84-87	90-93
COLOR (GSA NO.)	5GY4/1	5GY4/1	5GY4/1	5GY4/1	5GY4/1	5GY4/1	5GY4/1	5GY4/1	5GY4/1	5GY4/1	5GY4/1
ODOR	H2S	H2S	H2S	H2S	H2S	H2S	H2S	H2S	H2S	H2S	H2S
BULK WET DENSITY (PCF)		99999.		101.		103.		105.		100.	
VANE SHEAR STRENGTH (PSF)	99999.		34.		133.		163.		147.		319.
REMOLDED STRENGTH (PSF)	9.		24.		100.		58.		77.		91.
SENSITIVITY	9999.9		1.5		1.3		3.2		1.9		6.0
ORIGINAL WATER CONTENT (P)*		66.2		69.8		49.4		60.5		68.0	
SPECIFIC GRAVITY OF SOLIDS		2.71		2.71		2.71		2.69		2.71	
DRY DENSITY (PCF)		99999.		59.		69.		65.		60.	
VOID RATIO		999.99		1.85		1.46		1.57		1.84	
POROSITY (P)		9999.9		65.0		59.4		61.2		64.7	
SATURATED VOID RATIO		1.79		1.89		1.34		1.62		1.84	
LIQUID LIMIT (P)		66.		71.		51.		67.		79.	
PLASTIC LIMIT (P)		27.		33.		29.		29.		33.	
PLASTICITY INDEX		37.		38.		21.		38.		60.	
LIQUIDITY INDEX		106.		98.		85.		92.		87.	
COMPRESSION INDEX		.48		.55		.19		.48		.57	
CARBONATE CARBON CONTENT (P)		.34		.35		.18		.27		.50	
ORGANIC CARBON CONTENT (P)		.48		.49		.32		.52		.93	
SAND (P)		12.1		1.4		6.7		2.0		.5	
SILT (P)		35.2		35.9		48.6		45.6		36.7	
CLAY (P)		52.7		62.7		44.7		52.4		64.8	
ACTIVITY		.8		.7		.6		.8		.7	
MEDIAN DIAMETER (MM)		.0040		.0019		.0084		.0080		.0015	
SEDIMENT TYPE		SILTY CLAY		SILTY CLAY		CLAYEY SILT		SILTY CLAY		SILTY CLAY	
MICROSCOPIC ANALYSIS - PLUS 325 MESH FRACTION.(P)											
QUARTZ		80		70		85		75		55	
OTHER MINERALS		5		10		3		15		10	
MICA		5		15		10		5		5	
ORGANIC MATERIAL		5		2		1		2		TR	
SHELL FRAGMENTS		2		-		-		3		20	
FORAMINIFERA		2		3		1		TR		10	
SPICULES		1		TR		TR		TR		TR	
ASPHALT		TR		TR		TR		TR		-	
REMARKS***								TR		TR	

THE COLOR OF THIS SAMPLE IS A UNIFORM DARK GREENISH GRAY WITH SOME BLACK MOTTLED AREAS BETWEEN THE LINER AND THE SAMPLE. SAMPLE IS GENERALLY A SILTY CLAY WITH 3/4 INCH DIAMETER POCKETS OF SAND AT 5 AND 82 INCHES AND VERY SMALL SCATTERED POCKETS OF SAND IN INTERVALS 15-21 AND 40-53 INCHES. FEW VERY SMALL SHELL FRAGMENTS IN 1-9 INCH INTERVAL. TOP 9 INCHES HIGHLY DISTURBED DUE TO CRUSHING OF THE LINER DURING SAMPLING. AT 35 INCHES, A CAVITY 3/8 INCH DIAMETER AND 1.5 INCHES LONG APPEARS TO HAVE BEEN CONSTRUCTED BY A BURROWING ANIMAL. AT 46 INCHES, A 1/8 INCH HORIZONTAL SEPARATION OF THE SAMPLE IS PRESENT.

Table A 7 Summary of Test Results for Core 33 in Gulf of Mexico

[illegible]	[illegible]	WATER DEPTH [illegible] FT							
INTERVAL (IN)	[illegible]	[illegible]	[illegible]	[illegible]	[illegible]	[illegible]	[illegible]	[illegible]	[illegible]
BULK WET DENSITY (PCF)	9999.	1[illegible].	1[illegible].	1[illegible].	1[illegible].	1[illegible].	[illegible]	[illegible]	9[illegible].
VANE SHEAR STRENGTH (PSF)	9999.	1[illegible].	111.	159.	[illegible]	265.	[illegible]	260.	
REMOLDED STRENGTH (PSF)	17.	12.	55.	65.	[illegible]	71.	[illegible]	80.	
SENSITIVITY	9999.9	9.0	2.0	2.6	[illegible]	3.7	[illegible]	3.1	
ORIGINAL WATER CONTENT (P)*	[illegible]	76.1	71.1	47.6	67.5	[illegible]	71.6	[illegible]	71.0
SPECIFIC GRAVITY OF SOLIDS	[illegible]	2.72	2.72	2.69	2.69	[illegible]	2.71	[illegible]	2.72
DRY DENSITY (PCF)	[illegible]	9999.	59.	74.	61.	[illegible]	59.	[illegible]	56.
VOID RATIO	[illegible]	999.99	1.88	1.26	1.75	[illegible]	1.88	[illegible]	2.01
POROSITY (P)	[illegible]	9999.9	65.3	55.8	63.7	[illegible]	65.3	[illegible]	67.1
SATURATED VOID RATIO	[illegible]	2.06	1.99	1.28	1.82	[illegible]	1.94	[illegible]	2.04
LIQUID LIMIT (P)	[illegible]	68.	70.	69.	72.	[illegible]	70.	[illegible]	72.
PLASTIC LIMIT (P)	[illegible]	28.	26.	24.	20.	[illegible]	29.	[illegible]	31.
PLASTICITY INDEX	[illegible]	40.	44.	24.	52.	[illegible]	41.	[illegible]	41.
LIQUIDITY INDEX	[illegible]	121.	107.	95.	91.	[illegible]	105.	[illegible]	107.
COMPRESSION INDEX	[illegible]	.52	.54	.35	.56	[illegible]	.54	[illegible]	.56
CARBONATE CARBON CONTENT (P)	[illegible]	.42	.47	.55	.34	[illegible]	.42	[illegible]	.42
ORGANIC CARBON CONTENT (P)	[illegible]	.46	.37	.27	.48	[illegible]	.34	[illegible]	.53
SAND (P)	[illegible]	12.2	3.6	8.1	2.0	[illegible]	1.0	[illegible]	1.0
SILT (P)	[illegible]	32.5	38.2	54.2	33.0	[illegible]	32.0	[illegible]	34.8
CLAY (P)	[illegible]	55.4	58.2	37.7	64.1	[illegible]	67.0	[illegible]	64.2
ACTIVITY	[illegible]	.8	.9	.8	1.0	[illegible]	.7	[illegible]	.8
MEDIAN DIAMETER (MM)	[illegible]	.0028	.0024	.0134	.0016	[illegible]	.0014	[illegible]	.0015
SEDIMENT TYPE	[illegible]	SILTY CLAY	SILTY CLAY	CLAYEY SILT	SILTY CLAY	[illegible]	SILTY CLAY	[illegible]	SILTY CLAY
MICROSCOPIC ANALYSIS - PLUS 325 MESH FRACTION(P)									
QUARTZ	[illegible]	85	70	85	50	[illegible]	60	[illegible]	70
OTHER MINERALS	[illegible]	5	5	2	20	[illegible]	10	[illegible]	10
MICA	[illegible]	5	5	5	10	[illegible]	20	[illegible]	15
FORAMINIFERA	[illegible]	4	10	2	10	[illegible]	7	[illegible]	5
SPICULES	[illegible]	TR	5	1	5	[illegible]	TR	[illegible]	TR
SPONGE	[illegible]	TR	TR	TR	3	[illegible]	TR	[illegible]	TR
ORGANIC MATERIAL	[illegible]	TR	5	3	2	[illegible]	1	[illegible]	TR
SHELL FRAGMENTS	[illegible]	-	-	-	-	[illegible]	2	[illegible]	TR
ASPHALT	[illegible]	-	TR	2		[illegible]		[illegible]	

REMARKS***
THIS SAMPLE IS A DARK GREENISH GRAY SILTY CLAY WITH SEVERAL LAYERS AND POCKETS OF FINE SAND. THE LAYERS ARE ALL HORIZONTAL AND OCCUR IN INTERVALS 65-67. 69-69.5. AND 71-71.3 INCHES. A VERY THIN LAYER OCCURS AT 76 INCHES. LARGE POCKETS OF SAND APPROXIMATELY 3/4 INCHES IN DIAMETER ARE PRESENT AT 18.5 AND 79 INCHES. SMALL SCATTERED POCKETS OCCUR IN INTERVAL 23-56 INCHES. THE TOP 21 INCHES APPEARS DISTURBED DUE TO THE CRUSHING OF LINER DURING SAMPLING. SOME SMALL SHELL FRAGMENTS PRESENT IN INTERVAL 15-19 INCHES. SCATTERED BLACK MOTTLING IS VISIBLE BETWEEN LINER AND SAMPLE.

Table A-8. Properties of Seal Beach Testing Soil.

****** CORE NO DEMI - 1 ******

LATITUDE 34 6.00 N LONGITUDE 119 6.00 W WATER DEPTH 0. FT

INTERVAL (IN)	3- 6
COLOR (GSA NO.)	N2
ODOR	H2S
BULK WET DENSITY (PCF)	102.
VANE SHEAR STRENGTH (PSF)	16.
REMOLDED STRENGTH (PSF)	9.
SENSITIVITY	1.7
ORIGINAL WATER CONTENT (P)*	69.1
SPECIFIC GRAVITY OF SOLIDS	2.67
DRY DENSITY (PCF)	64.
VOID RATIO	1.63
POROSITY (P)	61.9
SATURATED VOID RATIO	1.61
LIQUID LIMIT (P)	43.
PLASTIC LIMIT (P)	25.
PLASTICITY INDEX	18.
LIQUIDITY INDEX	193.
COMPRESSION INDEX	.30
SAND (P)	35.8
SILT (P)	38.0
CLAY (P)	26.2
ACTIVITY	.9
MEDIAN DIAMETER (MM)	.0261
SEDIMENT TYPE	SAND SILT CLAY

Table A-9. Properties of Muqu Soil.

****** CORE NO REQD - 1 ******

LATITUDE 0 0.00 N	LONGITUDE 0 0.00 W
INTERVAL (IN)	0- 3
COLOR (GSA NO.)	5Y4/1
ODOR	H2S
BULK WET DENSITY (PCF)	95.
VANE SHEAR STRENGTH (PSF)	17.
REMOLDED STRENGTH (PSF)	10.
SENSITIVITY	1.7
ORIGINAL WATER CONTENT (PI)*	77.6
SPECIFIC GRAVITY OF SOLIDS	2.73
DRY DENSITY (PCF)	54.
VOID RATIO	2.18
POROSITY (P)	68.6
SATURATED VOID RATIO	2.12
LIQUID LIMIT (P)	58.
PLASTIC LIMIT (P)	31.
PLASTICITY INDEX	27.
LIQUIDITY INDEX	173.
COMPRESSION INDEX	.43
SAND (P)	9.3
SILT (P)	42.1
CLAY (P)	48.6
ACTIVITY	.5
MEDIAN DIAMETER (MM)	.0155
SEDIMENT TYPE	SILTY CLAY

Appendix B

FIELD TEST PROCEDURES IN THE GULF OF MEXICO

by

G. M. Dunn and F. L. Rose

TEST SITE AND OPERATIONS

The third phase of the Deep Submergence Systems Project (DSSP)-NCEL bottom breakout force tests was conducted in the Gulf of Mexico, the test site chosen by a field survey conducted by NCEL during March 1967. In accordance with the findings of the survey, the tests were performed within the southern half of block 212 of the Eugene Island area.

The 155-foot-long by 36-foot-wide supply class vessel *Caribe Tide* provided the working platform from which to conduct the tests at sea. Approximately 3,000 ft^2 of deck space was arranged with equipment as shown in Figure B-1. In order to perform uninterrupted test operations the *Fast Tide*, a 65-foot-long by 22-foot-wide vessel, transported supplies and personnel to the test site, approximately 90 miles from Morgan City, Louisiana, the nearest port.

Personnel required to perform the necessary operations for testing at sea comprised a 16-man complement to the *Caribe Tide*. These personnel were assigned as follows:

Vessel crew members (5)
Riggers (3)
Crane operator
Divers (5)
Engineering technician
Resident project engineer

The vessel crew, crane operator, and two riggers were furnished by the contractor; one rigger, and engineering technician, and the resident project engineer were assigned by NCEL; the five Navy divers were assigned by the DSSP Technical Office, San Diego.

A dawn-to-dusk working day was necessary to complete a maximum number of tests, which was limited by allowable diving "bottom time," settlement periods, and weather. Personnel were assigned errands and duties as required ashore to avoid fatigue and maintain morale.

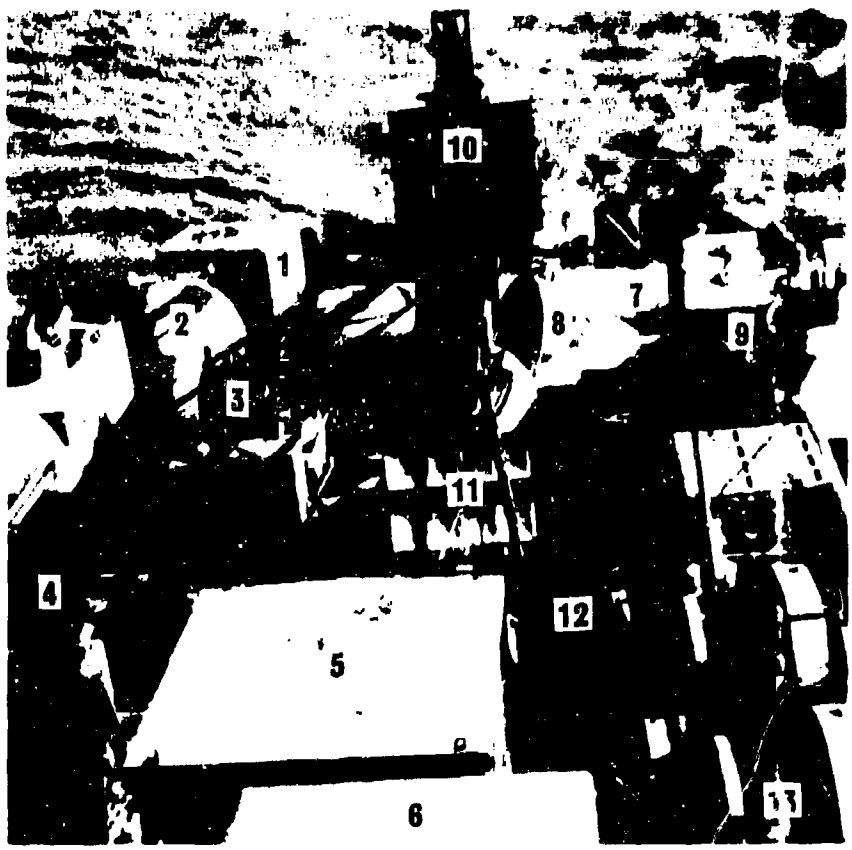

1. cube
2. sphere
3. aft mooring winch
4. 125-cfm air compressor
5. instrument shack
6. personnel quarters
7. cylinder
8. cone
9. parallelepiped
10. 45-ton crane
11. STATO anchors
12. pontoons
13. BU 140 mooring winch

Figure B-1. Equipment and apparatus secured to the deck of the *Caribe Tide*. The heavy test objects were clustered around the crane to facilitate lowering them over the stern.

The test site was located by triangulation by turning horizontal sextant angles with respect to known locations of local oil platforms. The ship's radar was used to verify the approximate position.

In order to maintain position during a test the vessel was held in a two-point moor by means of the 6U 140 winches shown in Figure B-1. A 12,000-pound STATO anchor was fairleaded at the bow to provide positive location control for the entire testing period. Placement of a 3,000-pound lightweight (LWT) Navy anchor from the stern allowed the vessel to be positioned in a catenary adjacent to the test site for performance of the test operations. At the end of a day's testing the smaller stern anchor was easily drawn up to allow bow mooring into the seas for personnel comfort. The mooring cable consisted of 1,800-foot lengths of 1-1/4-inch-diameter, 6 x 19 IPS (improved plow steel) wire rope.

A 100-foot-long cable pendant was shackled between the mooring cable and the 30-foot-long, 2-inch-diameter chain attached to the STATO anchor. The shackle connecting the two cables was cut to free the vessel of its moor in heavy seas. A 3/4-inch-diameter buoy cable, attached at the point of severance, provided a rapid means of recovering the pendant when the storm subsided.

An auxiliary length of cable on the second drum of the aft winch provided a means of lifting heavy loads to the surface within reach of the 45-ton crane. This line was fairleaded over a stern roller which transmitted the stresses directly to the hull of the vessel. This lifting method was utilized during the initial lowering and retrieval of the test objects as well as for retracting the STATO anchor at the termination of the test operations. A constant load, augmented by the rocking of the vessel, loosened the anchor from the mud.

The weight of the test objects, the heaviest loads to be lifted at sea, approached the safe design capacity of the crane. Thus, they were located aft, close to the crane, so that they could be lowered over the stern to minimize the rolling effects of the vessel. The instrumentation shack was centrally located on deck so that all operations could be closely monitored. This location was advantageous in that visual observation was unobstructed and voice communication was sufficient to coordinate activity.

At-sea operations were often made hazardous by weather conditions. Because of the tremendous weight of the test objects, they were lifted from the deck only during calm sea states. A typical lifting situation, as shown in Figure B-2, was prohibited if sea conditions imparted even a gentle roll to the work vessel. Diving operations and tests were limited only by the sea conditions under which the 3,000-pound LWT anchor would not hold firmly. Divers would enter and exit the water from the lee side of the vessel to avoid the swells as much as possible.

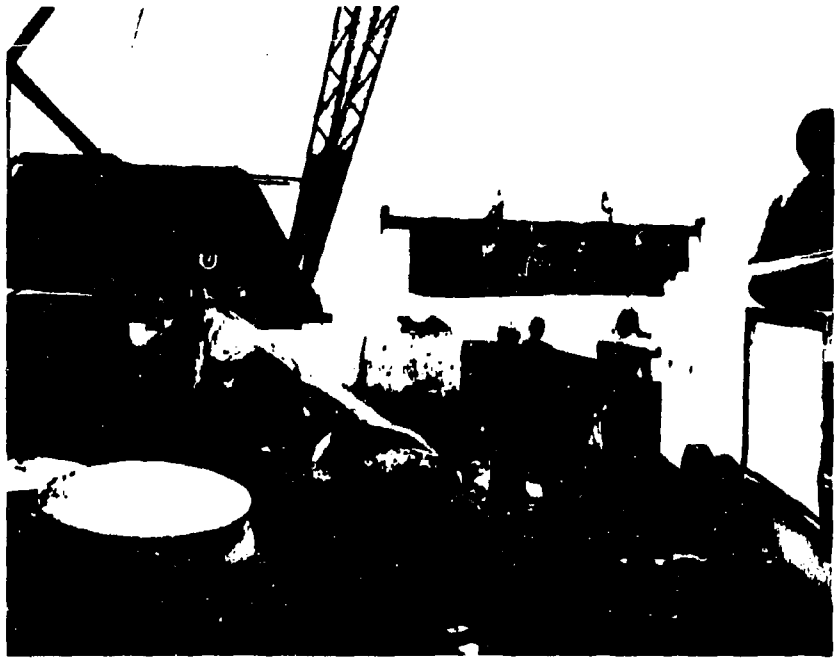

Figure B-2. Test object being lifted from the deck.

TEST APPARATUS

Each of the five test objects were fitted with a wire rope bridle (1-1/4-inch, 6 x 19 IPS) so that the line of action of the lifting force would pass through the object's center of gravity. Placement of an object on the bottom involved several operations. The object was first raised from the deck with the crane and positioned in the water at the stern. The auxiliary line from the aft mooring winch was then shackled to the wire rope bridle to assume the load, and the crane line was disconnected. A buoy line (3-foot-diameter steel buoy on 3/4-inch-diameter 6 x 19 IPS wire rope cable) was attached to a pad eye on the object, which was then lowered to the bottom. Two scuba divers disconnected the aft winch line from the object to complete the procedure.

Two 8.4-ton rubber collapsible (salvage) pontoons[8] were connected in series to impart, when inflated, an uplifting force to the object. A schematic of the lifting line assembly is shown in Figure B-3. The entire line was assembled aboard the vessel, lowered over the side adjacent to the buoy line, and attached to the object. The top pontoon was inflated only enough to maintain the attitude of the lifting line with the bottom pontoon deflated.

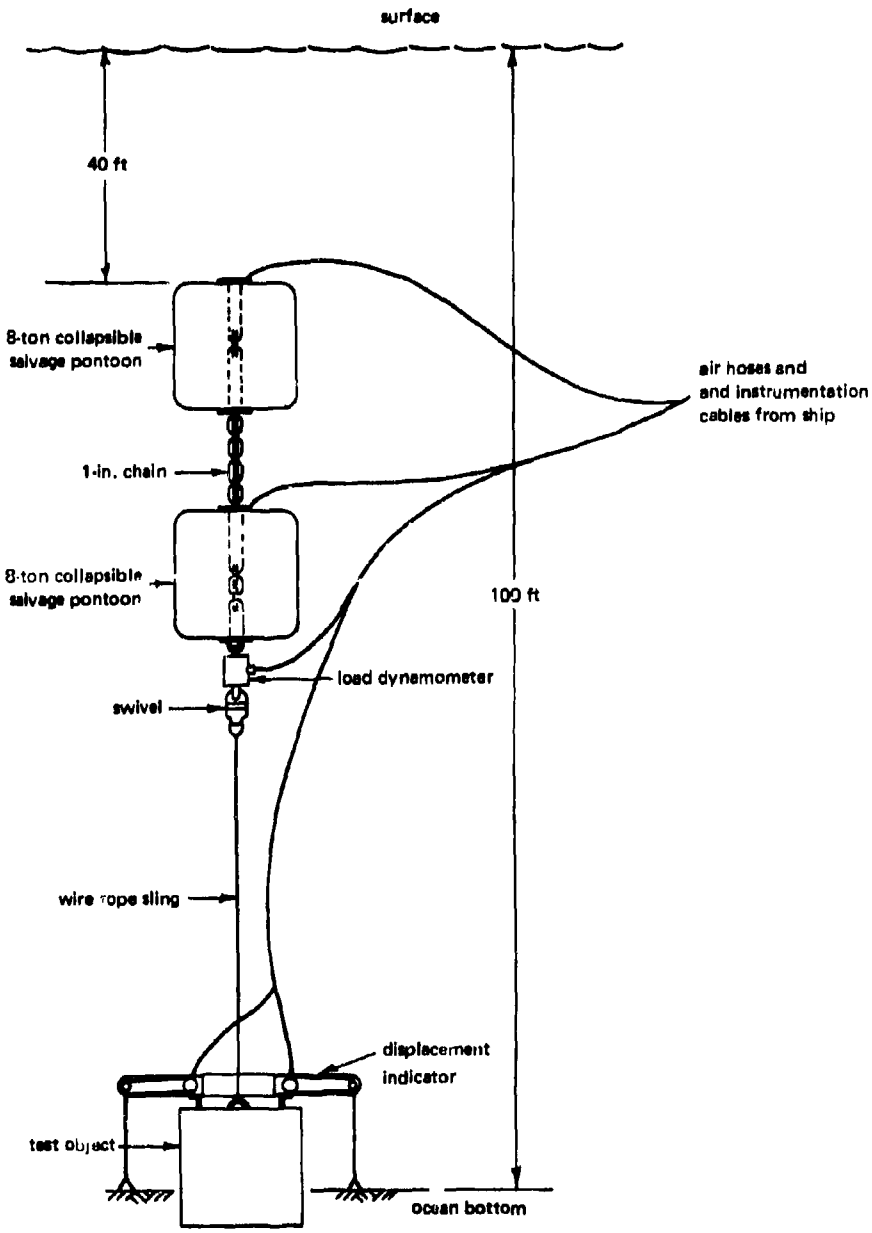

Figure B-3. Lifting line assembly and instrumentation.

The experimental procedure dictated that the test object be allowed to settle into an undisturbed area on the bottom. During this settlement period, the test site was marked by the buoy at the surface and left unattended. No fouling of the lifting line assembly and buoy line was experienced during this period, even though waves ranged from 12 to 18 feet during the frequent winter storms.

TEST PROCEDURES

Settlement Test

A test was conducted to determine the minimum length of time that an object must be undisturbed to reach nearly its maximum settlement into the bottom. During the test, settlement was monitored with the displacement indicator. The indicator measured movement of the object relative to the bottom and was calibrated to measure directly the depth of settlement. The indicator was attached to the object by divers immediately after the object was disconnected from the aft winch lowering line.

The pontoon lifting line was then attached, and the top pontoon was inflated only enough to maintain attitude. The effect of swells and waves on the lifting assembly and buoy was then monitored by the load dynamometer during the test. This sinuous load was quite small in magnitude and did not perceptibly influence the settlement of the object.

The instrumentation cable attached to the displacement indicator and load dynamometer was the only physical connection between the test apparatus and the surface vessel. Divers inspected the site periodically to observe the pontoon line and also warn against the unexpected settlement of the displacement indicator reference weights.

Breakout Test

A breakout test consisted of extracting an object from the mud bottom after it had been allowed to settle to equilibrium. Since the lifting line was already attached to the object, very few preparations were required prior to conducting the test. Divers connected the instrumentation cable to the load dynamometer and displacement indicator, and continuity was checked from the instrument shack. In-situ vane shear strength was measured, and the settlement of the object was inspected. The final diving operation was to connect the air inflation hoses to the pontoon and open all valves. Air was then forced into the pontoons by a 125-ft^3/min compressor to develop a

predetermined uplifting force which was monitored by the load dynamometer. Upon reaching the required force, air valves were secured at the compressor, and the force was maintained constant throughout the test.

The climax of a test came when the object was extracted from the mud bottom, which was indicated by the surfacing of the top pontoon, as shown in Figure B-4. A 1-inch-diameter polypropylene line attached to the top pontoon prevented the entire assembly from drifting away.

The pontoons were deflated by "bleeding" air from them until the object had once again been placed on the bottom for settlement and only enough air remained in the top pontoon to maintain attitude. All air lines were secured and disconnected by the divers, and instrumentation cables were retrieved. After an inspection by the divers the object was allowed to settle at the new test site.

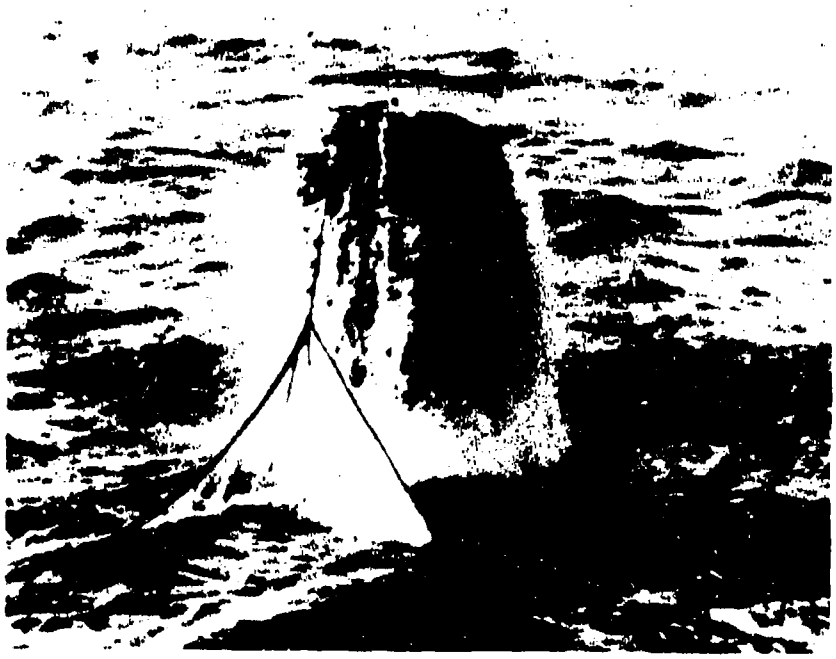

Figure B-4. Pontoon surfaces, indicating breakout.

Data Acquisition

Electronic data were originated from both the load dynamometer and the displacement indicator. The load dynamometer consisted of a strain gage bridge which measured a variation in strain which was calibrated to a corresponding tensile force. The displacement indicato consisted of a mechanical linkage associating linear displacement with variable resistance. These data were recorded using system D amplifiers and an oscillograph. A facsimile of the recorded data is shown in Figure B-5. The in-situ vane shear test was performed by divers with a 4-inch by 8-inch vane and a torque wrench which measured maximum applied torque before shearing. A simple conversion was required to convert the in.-lb measurement to psi.

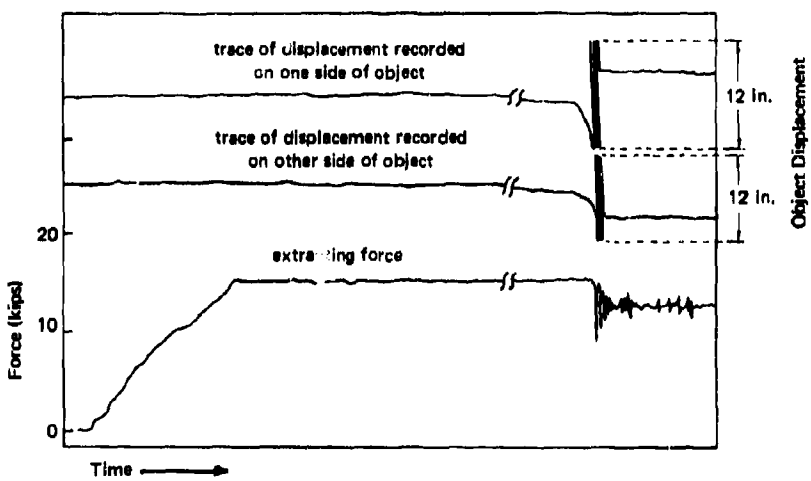

Figure B-5. Facsimile of recorded data.

REFERENCES

1. Naval Civil Engineering Laboratory. Technical Note N-863: Breakout forces, by B. J. Muga. Port Hueneme, Calif., Sept. 1966. OUO

2. ——. Technical Report R-591: Ocean bottom breakout forces, including field test data and the development of an analytical method, by B. J. Muga. Port Hueneme, Calif., June 1968. (AD 837647L)

3. Southwest Research Institute. Report on Contract N-Onr-336300: Force required to extract objects from deep ocean bottom, by R. C. DeHart and C. R. Ursell. San Antonio, Tex., Sept. 1967. (AD 658757)

4. Private correspondence with A. S. Vesić, Professor of Civil Engineering, Duke University, Durham, N. C., Feb. 16, 1968.

5. Naval Civil Engineering Laboratory. Technical Report R-537: In-situ, sea-floor plate bearing device: A performance evaluation; including data on the short-term load-settlement response of cohesive and noncohesive bottom sediments, by T. R. Kretschmer. Port Hueneme, Calif., June 1967. (AD 654714)

6. ——. Technical Report R-503: Engineering properties of marine sediments near San Miguel Island, California, by M. C. Hironaka. Port Hueneme, Calif., Dec. 1966. (AD 644192)

7. ——. Technical Report R-566: Computer reduction of data from engineering tests on soils and ocean sediments, by M. C. Hironaka. Port Hueneme, Calif., Feb. 1968. (AD 666311)

8. Naval Ships Systems Command. NAVSHIPS 0994-011-2010: Pontoon-Salvage. Washington, D. C., Jan. 1967.

NOMENCLATURE

A	Object surface area under soil (in.^{2})
A_m	Maximum cross-sectional area of object under soil (in.^{2})
A_s	Side surface area of failure prism (in.^{2})
A_x	Base surface area of failure prism (in.^{2})
B	Buoyancy of test object (lb)
B_s	Soil buoyancy force (lb)
B_w	Water buoyancy force (lb)
C	Damping coefficient
c	Soil cohesion; undrained shear strength (psi)
C_1, C_2	Constants
C_s	Shape factor
D	Original embedment depth (in.)
D'	Dynamic damping
e	Eccentricity
F	Net breakout force or soil holding strength (lb)
F_a	Applied lifting force (lb)
F_m	Mean value of the estimated soil holding strength (lb)
F_r	Soil resistance (lb)
F_{rb}	Soil bearing resistance (lb)
F_{rs}	Soil shear resistance (lb)
F_{rt}	Soil tension resistance (lb)
$F(t)$	Forcing fun·
h	Depth of we
K	Spring consi
k	Permeability
M	Mass (slug)
m	Mass of obje
m'	Virtual mass
n_1, n_2	Constants
P	Perimeter of
p	Hydrostatic
q_d	Average sup soil to main static equilil
R	Resultant fc
T	Breakout tir
T_e	Effective br·
T_{in}	Time of obj
t	Time (min)
V_s	Volume of s
W	Dry weight
W_w	Weight of ol
X, Y	Variables
y	Displacemei

$F(t)$	Forcing function (lb)
h	Depth of water above soil (ft)
K	Spring constant
k	Permeability
M	Mass (slug)
m	Mass of object (slug)
m'	Virtual mass (slug)
n_1, n_2	Constants
P	Perimeter of failure prism (in.)
p	Hydrostatic pressure (psi)
q_d	Average supporting pressure provided by the soil to maintain the embedded object in static equilibrium (psi)
R	Resultant force (lb)
T	Breakout time (min)
T_e	Effective breakout time (min)
T_{in}	Time of object embedment (min)
t	Time (min)
V_s	Volume of soil displaced by object (ft^3)
W	Dry weight of object (lb)
W_w	Weight of object in water (lb)
X, Y	Variables
y	Displacement (in.)
y'	Velocity, dy/dt
y''	Acceleration, d^2y/dt^2
y_b	Displacement at breakout (in.)
γ	Specific weight of water (lb/ft^3)
γ_s	Specific weight of saturated soil (lb/ft^3)
δ	Mean grain size (in.)
ϵ	Surface roughness (in.)
μ_w	Viscosity of water (lb-sec/ft^2)
μ_s	Viscosity of soil (lb-sec/ft^2)
ρ_w	Density of water ($slug/ft^3$)
ρ_s	Density of soil ($slug/ft^3$)
σ	Soil bearing strength (psi)
σ_t	Soil tension strength (psi)
ϕ	Angle between a horizontal plane and the elemental surface area of an object (deg)

13

Unclassified
Security Classification

DOCUMENT CONTROL DATA - R & D

Security classification of title, body of abstract and indexing annotation must be entered when the overall report is classified)

1 ORIGINATING ACTIVITY (Corporate author) Naval Civil Engineering Laboratory Port Hueneme, California 93041	2a. REPORT SECURITY CLASSIFICATION Unclassified 2b. GROUP

3 REPORT TITLE

OCEAN SEDIMENT HOLDING STRENGTH AGAINST BREAKOUT OF EMBEDDED OBJECTS

4 DESCRIPTIVE NOTES (Type of report and inclusive dates)
Final; July 1967 – July 1968

5 AUTHOR(S) (First name, middle initial, last name)
Cheng L. Liu

6 REPORT DATE	7a. TOTAL NO OF PAGES	7b. NO OF REFS
August 1969	71	8

8a. CONTRACT OR GRANT NO	9a. ORIGINATOR'S REPORT NUMBER(S)
b. PROJECT NO 56-001	TR-635
c.	9b. OTHER REPORT NO(S) (Any other numbers that may be assigned this report)
d.	

10 DISTRIBUTION STATEMENT
This document has been approved for public release and sale; its distribution is unlimited.

11 SUPPLEMENTARY NOTES	12 SPONSORING MILITARY ACTIVITY
	Deep Submergence Systems Project Office 6900 Wisconsin Avenue Chevy Chase, Maryland 20015

13 ABSTRACT

This report concludes 3 years of breakout force research. The third phase of the field test conducted in the Gulf of Mexico and a small-scale model study are described. All of the experimental results are presented in a new dimensionless correlation (between breakout force and breakout time) based on the mechanism of the breakout. The mean soil holding strength (F_m) is considered to depend upon average soil cohesion, object geometry, the time the object has been embedded (T_{in}), and the time allowed for pullout (T):

$$\frac{F_m}{F_r} = 1.5 \left(\frac{T}{T_{in}}\right)^{-0.07} \qquad \text{for } 10^{-3} < T/T_{in} < 10$$

where F_r is the static soil resistance due to shear and tension. An example is also presented to illustrate the application of this equation. The small-scale model test is considered a useful tool in obtaining more data in future research.

DD FORM 1 NOV 65 1473 (PAGE 1)
S/N 0101-807-6801

Unclassified
Security Classification

14 KEY WORDS	LINK A		LINK B		LINK C	
	ROLE	WT	ROLE	WT	ROLE	WT
Breakout force						
Field tests						
Ocean sediment						
Breakout time						
Model tests						
Breakout mechanism						